THE IMPACTION OF AIRBORNE PARTICLES ON PLATE COLLECTORS

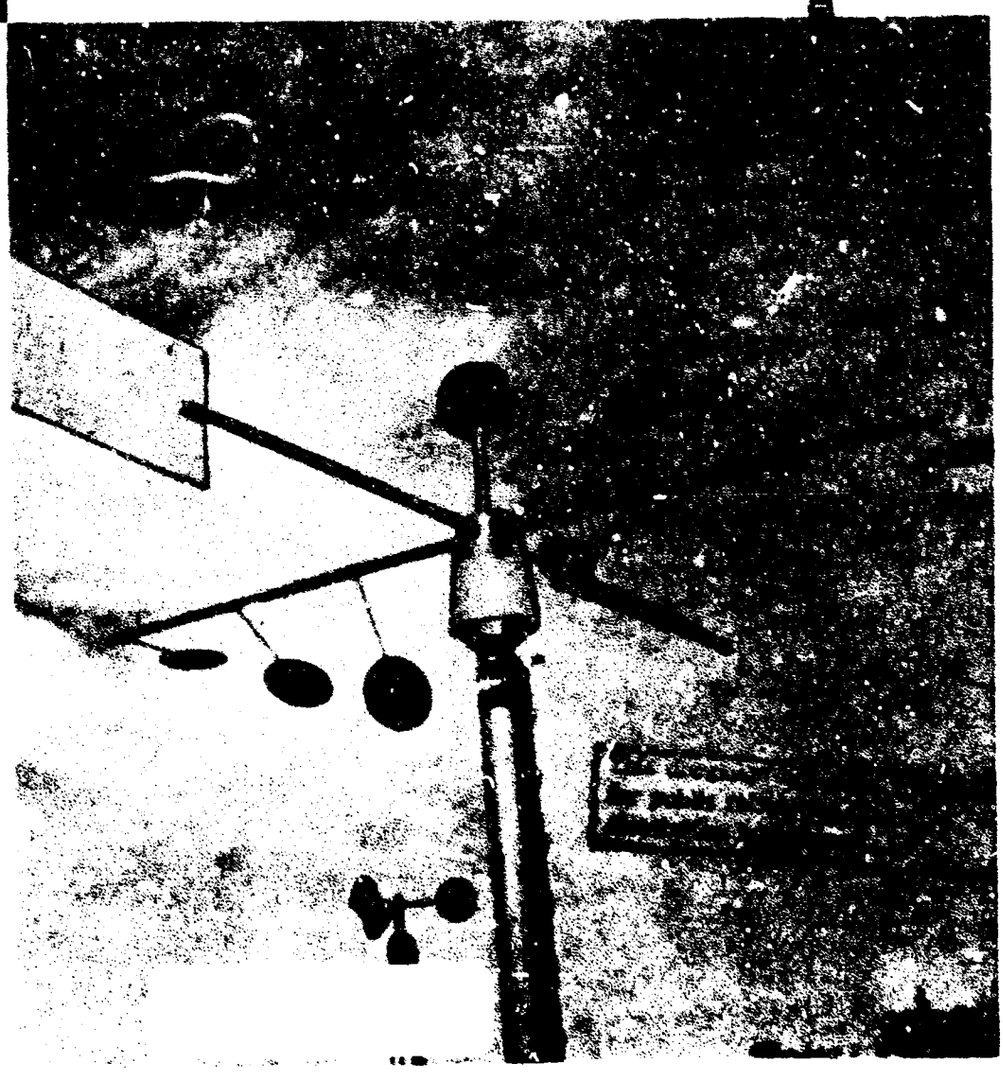

STANFORD
RESEARCH
INSTITUTE

MENLO PARK
CALIFORNIA

THE IMPACTION OF AIRBORNE PARTICLES ON PLATE COLLECTORS

OCD Work Unit No. 3119A

SRI

THE IMPACTION OF AIRBORNE PARTICLES ON PLATE COLLECTORS

SRI Project
No. MU-6358

By:

Carl F. Miller

Contract No. NOO22867C1143
OCD Work Unit No. 3119A

April 1967

STANFORD
RESEARCH
INSTITUTE

MENLO PARK
CALIFORNIA

Prepared for:

OFFICE OF CIVIL DEFENSE
DEPARTMENT OF THE ARMY
WASHINGTON, D.C.

Through:

Technical Management Office
U.S.N.R.D.L.
San Francisco, California

CONTENTS

ILLUSTRATIONS

TABLES

INTRODUCTION

The impaction on and retention by surfaces of all kinds of airborne particles are the source of a variety of peacetime problems ranging from persistent cleaning chores for housewives to serious air pollution threats to whole urban areas. A dramatic example of the latter kind of problem concerned the city of San José, Costa Rica, when volcano Irazú began erupting in March 1963 and ejected huge quantities of sand-like particles that were carried by the winds and fell on the city and surrounding countryside.

This report on the impaction of airborne particles on plate collectors discusses data that were obtained from a plate collector that was designed for use in Costa Rica in support of field experiments on the retention of the volcanic particles by the foliage of plants. The major purpose in obtaining these data was to improve the data base for evaluating an even more serious possible future problem: the consequences of fallout from nuclear explosions in the event of nuclear war.

The field experiments in Costa Rica and the circumstances under which the plate collector was used are described in the reports on Operation Ceniza-Arena.[1,2,3] Portions of these reports are repeated along with the necessary extensions for describing the methods by which the data were analyzed.

BACKGROUND

The interception of airborne particles by plant parts, such as leaves or stems, or by other objects is often evaluated in terms of the impaction coefficient, η. The impaction coefficient is defined as the ratio of the number of particles that impact on the surface of the object to the number of particles in the air volume swept by the object.

The two main mechanisms involved in the interception of falling particles by surfaces of simple objects are impaction by inertia from a moving airstream and impaction by settling caused by gravitational force. Impaction by inertia is the predominating mechanism by which the very small particles on a moving airstream make contact with a surface. At a given velocity of the airstream, particles with diameters smaller than a given diameter will not impact; they will follow the airstream around the object. According to the theory and data of Ranz and Wong[4], the value of η for impaction by inertia on discs and cylinders having a diameter of about 1 inch becomes zero for particles with diameters less than about 20 microns in an airstream moving with a speed of about 3 feet per second.

Impaction by gravity settling is the predominating mechanism by which the larger particles make contact with a surface, given a constant wind speed. For a given particle size, the gravity-settling mechanism becomes more important as the wind speed decreases. The value of η for impaction by settling approaches unity for particles whose falling velocity is about equal to the wind speed. For a wind speed of about 3 feet per second, the particle diameter for an impaction coefficient of unity would be between 150 and 200 microns.

In essentially all environmental situations entailing the impaction and retention of airborne particles, both mechanisms of impaction are combined since the particles generally are mixed with respect to size and many have diameters that are intermediate with respect to the limits given for the two impaction mechanisms. Theoretical equations for the combined impaction mechanisms and for variable distributions of particle diameters have not yet been reported.

The role of the impaction coefficient in the interception and retention of airborne particles by objects may be illustrated mathematically

by the following definition of the contamination factor for a plant part (such as a leaf)

$$a_L(\alpha_p) \quad \epsilon_o(\alpha)(1 + \alpha_p^2)^{1/2} S_L(\alpha_p) \eta F(w_L) \tag{1}$$

in which

$\epsilon_o(\alpha)$ is the initial retention coefficient for a particle size-group, designated by α, which hit a plant surface

α_p is the land-surface value of γ ($\alpha_p = v_w^o / v_f^o$, where v_w^o is the surface wind speed and v_f^o is the terminal, or falling, velocity at the plant of the particle size-group designated by α)

$S_L(\alpha_p)$ is the projected specific surface area of the foliage (i.e., plant area per unit plant weight) in a plane normal to the particle flux

η is the particle impaction coefficient caused by interception and inertia

and

$F(w_L)$ is the dilution function whose value depends on the planting density or the average foliage surface density.

The experimental measurements, designed to provide separate information on the impaction coefficient, consisted in the collection of particles on greased plates that were set at a series of angles, θ, from the horizontal; the plane of the plates was kept perpendicular to the direction of wind by mounting the collecting system with an attached wind vane on a swivel bearing. The grease film on the surface of the plates was used to assure that the value of the retention coefficient for all plates would be one. After an exposure to depositing particles, the weight of the collected particles was measured; this weight, after making a correction for background dust, is designated as m (in grams per square foot). During the exposure, the average wind speed over the collecting period, designated as $\bar{v}_w$ (in feet per second), was measured with a hand-held calibrated anemometer.

The basic assumptions used in the relationships described below include: (1) for a given exposure or set of measurements of m, the range of particle diameters in the collected deposits was small, so that the terminal fall velocity of the particles could be represented by an

average value designated as $\bar{v}_f^o$; (2) the wind speed during the time that the particles impacted was near the value of $\bar{v}_w^o$; (3) the lag time of the wind vane was small relative to the time rate of change in the wind direction; and (4) the value of the impaction coefficient depends on plate angle, particle fall velocity, and wind speed (for a given plate diameter).

To minimize the collection of particles with a broad range of diameters, large or extreme changes in wind speed, and overloading of the greased plates, short exposure periods were desired. On the other hand, some extended time was required to collect a sufficient quantity of particles whose weight was significantly greater than the weight of the background dust.

Using these assumptions, the basic relationship for defining the impaction coefficient, η, is given by

$$m = \eta m_a \sin(\theta - \bar{\varphi}) \tag{2}$$

in which m_a is the integrated particle flux across a plane perpendicular to the average fall vector, and $\bar{\varphi}$ is the average angle of fall of the particles at the height of the collector plates (measured from the horizontal in the direction of the wind). The average terminal fall velocity of the collected particles is given by

$$\bar{v}_f^o = \bar{v}_w^o \tan \bar{\varphi} \tag{3}$$

The average air concentration of the particles for the exposure period is given by

$$\bar{C}_a = m_a / (\bar{v}_f^o t) \tag{4}$$

where t is the exposure time. The values of θ, fixed by the design of the collector (see Experimental Procedures), were 0, 30, 60, 90, 120, 150, and 180 degrees. The values of m for each plate, $\bar{v}_w^o$, and t were measured.

The angular arrangement of the collector plates, in which the plate angles vary from 0 to 180 degrees, produces four general classes of relative geometries for impaction of falling particles in a horizontal wind stream; these are as follows:

1. Plate angles between 90 and 180 degrees; both the air and the particles strike the top or front face of the plates.

2. Plate angles less than $\bar{\varphi}$; the air strikes the bottom of the plates, and the majority of the impacting particles strike the top of the plates.

3. Plate angles greater than $\bar{\varphi}$ but less than 90 degrees; the air and particles strike the bottom of the plates.

4. An extension to the third class; a small number of particles may deposit on the top side of the plates at angles between $\bar{\varphi}$ and 90 degrees because of turbulence in the airflow over and around the plates.

Generally, the plate that is set at an angle, θ, of 90 degrees from horizontal would be expected to cause a greater diversion of the airstream than would one set at any other angle (assuming the airstream moves parallel with the surface of the ground). However, the degree of diversion of the airstream by a plate should not be expected to cause a proportionate diversion of the airborne particles, especially in terms of the weight of the collected particles. For example, if the angle of the plate is very near the angle of fall of a particle, only a small deflection in the falling trajectory could cause the particle to miss the plate. Larger particles (i.e., in the size range of concern in this study) that impact mainly by gravity settling would not be deflected as readily as would the smaller particles by the airflow around the plates. These two factors suggest that the plate set at an angle very nearly perpendicular to the angle at which the particles approach the collector should collect the largest fraction (per unit projected area) of the particles in the passing airstream.

If it is assumed, for the first class of geometries, that η has a maximum value at a plate angle, θ_o (which is about 90 degrees greater than $\bar{\varphi}$), and that fractional decreases in η are proportional to the angular displacement of the plate from θ_o, a first approximation of the dependence of η on the plate angle (because of the change in angle at which the wind strikes the plate) may be written as

$$\frac{d\eta}{\eta} = -2\gamma \sin 2(\theta - \theta_o)d(\theta - \theta_o) \qquad (5)$$

where γ is a proportionality constant whose value is assumed to depend on the average wind speed and on the average falling velocity of the particles. The factor of 2 is inserted to indicate that the sine function must vary a whole cycle for each 180-degree change in $\theta - \theta_o$ (i.e., the value of η must be the same at θ_o and at $\theta_o \pm 180$ degrees).

Integrating Equation 5 under the condition that η is equal to η^o when θ is equal to θ_o (i.e., η^o is the impaction coefficient for a plate that is set at the angle θ_o) gives

$$\ell n\ \eta/\eta^o = -\gamma\left[1 - \cos 2(\theta - \theta_o)\right] \qquad (6)$$

Combining Equation 6 with Equation 2 in logarithmic form gives

$$\ell n\ m = \ell n\ \eta^o m_a + \ell n \sin(\theta - \bar{\varphi}) - \gamma\left[1 - \cos 2(\theta - \theta_o)\right] \qquad (7)$$

If it is assumed that θ_o is 90 degrees larger than $\bar{\varphi}$ for all values of $\bar{v}_f^o$ and $\bar{v}_w^o$ of interest, Equation 7 can be written as

$$\ell n\ m = \ell n\ \eta^o m_a + \ell n \sin(\theta - \bar{\varphi}) - \gamma\left[1 + \cos 2(\theta - \bar{\varphi})\right] \qquad (8)$$

The value of γ represents the fractional decrease in η^o for plates at angles other than θ_o. If the diversion of the airflow patterns around the plates increases as the wind speed increases (as expected), the value of γ should increase as the wind speed increases. Because the diversion of the airflow should have a smaller effect on the impaction of the larger particles than on the smaller particles, the value of γ (for a given wind speed) should decrease as the value of $\bar{v}_f^o$ increases.

For the second class of geometries in which the particles strike the top of the plates (where $\theta \leq \bar{\varphi}$), geometric considerations suggest that η should increase as the value of $(\bar{\varphi} - \theta)$ increases. Since θ is always less than $\bar{\varphi}$, the area swept by a plate decreases as $(\bar{\varphi} - \theta)$ decreases; if it is assumed that the impaction coefficient, for a given wind speed or for a given value of $\bar{\varphi}$, is proportional to the cross-sectional area of the particle flux swept by the plate, then the impaction coefficient should be about proportional to sin $(\bar{\varphi} - \theta)$.

For the third class of geometries in which the particles strike the bottom of the plates (where $\theta \geq \bar{\varphi}$), geometric considerations suggest that η should approach zero as θ approaches zero degrees and should approach its maximum value as θ approaches 90 degrees. Thus η should be proportional to sin θ since this function varies from 0 to 1 as θ varies from 0 to 90 degrees. For a plate angle of 90 degrees or greater, the conditions for the first class of geometries apply. Also, the wind-particle flux geometric effects on the impaction coefficient should be similar to that for the direct impact of the particles for the second class of

geometries (even though the particles are striking the bottom rather than the top of the plate). If gravity plays a role in the mechanism, the value coefficients for the third class of geometries should be smaller than those for the second class. The two geometric considerations suggest that the impaction coefficient should be proportional to sin θ sin $(\theta - \bar{\varphi})$.

Although the fourth class of geometries requiring the impaction of particles on the top of the plates is indicated only for values of θ greater than $\bar{\varphi}$ in the above definitions, the effect on the impaction by air turbulence in back of each plate actually should apply to all values of θ between 0 and 90 degrees. Geometrical considerations suggest that the effect of turbulence should be nonexistent at θ equal to zero and should be proportional to the cross-sectional area of the airstream swept by the plate; thus, for turbulent effects, η should be proportional to sin θ. It also is expected that, for a given value of θ, η should decrease as $\bar{\varphi} - \theta$ increases when $\bar{\varphi}$ is greater than θ (for a given particle diameter and plate angle, an increase in $\bar{\varphi} - \theta$ can only result from an increase in wind speed). Conversely, η should increase as $\theta - \bar{\varphi}$ increases when $\bar{\varphi}$ is less than θ. (If θ and $\bar{v}_f^o$ are constant, $\theta - \bar{\varphi}$ can only increase if the wind speed decreases.)

If the terrain at the location is sloped and if the plate collector post and anemometer post are set perpendicular to level, a correction to the falling velocities is required. Since the air near the surface moves parallel to the ground, the effective falling velocity of the particles will be either greater or less than their true falling velocity if the direction of the wind is either down or up the slope of the terrain. If the downward component of the wind speed is designated as $\bar{v}_z$, then the average falling velocity of the particles is given by

$$\bar{v}_f = \bar{v}_w \tan \bar{\varphi} - \bar{v}_z \qquad (9)$$

EXPERIMENTAL PROCEDURES

A view of the plate collector is shown in Figure 1; the gross particle or tray collector is shown in Figure 2.

The collector plates consisted of 4-inch-diameter thin aluminum discs welded to 1/4-inch-diameter aluminum rods that were 6 inches long. The assembled collector consisted of seven plates mounted 8 inches apart on a 4-foot rod so that the plane of each plate was parallel to the rod but at angles of 0, 30, 60, 90, 120, 150 and 180 degrees from horizontal. The 4-foot rod was mounted on a swivel bearing with a wind vane to keep the center plate and rod perpendicular to the direction of the wind. The small rods holding the plates were threaded to accept hex nuts to facilitate installation on and removal from the main rod. Before installation, the plates were greased by brushing both sides with a 50-50 mixture of petroleum jelly and xylene; after the xylene evaporated, the plates were warmed until the grease softened to form a smooth thin film over the plate.

The particles were recovered from the plate, each side separately, by warming the plate and washing the grease and particles into beakers with a thin stream of xylene from a plastic wash bottle. The particles were collected on filter paper. After the filter paper was ashed in a muffle furnace, the particles were cooled to room temperature and weighed on an analytical balance.

The greased plates were transported between the laboratory in San José and the field in a dustproof box. When a cloud of ceniza-arena particles appeared to approach the land plot being manned, the plates were quickly mounted on the main rod under cover (in the jeep or a rain shack) and installed on a prepared post. The length of exposure of the plates, from the time of arrival of the particles to the recovery of the sampler, was measured with a stopwatch. The wind speed during the exposure was measured with a calibrated anemometer mounted on an adjacent post at the same height (8 feet) as the collector.

The tray collectors for making ground-level collections of the ceniza-arena were 2-foot-square aluminum trays with 2-inch walls. Thin aluminum louvers (like a venetian blind) that inclined at an angle of 45 degrees were inserted to minimize blow-out of small particles and

Figure 1

PLATE COLLECTOR

Figure 2

GROSS COLLECTOR

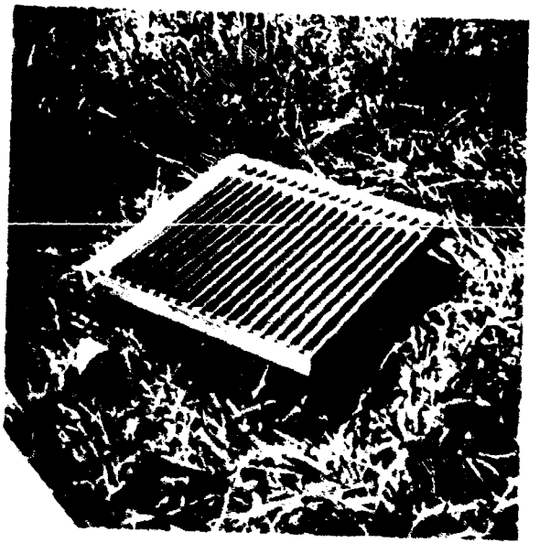

bounce-out of large particles. The louvers were held in position by placement in 45-degree angle slits that were cut into two aluminum metal strips; with the slit construction, the inserts could be completely disassembled for ease in recovering the collected particles. The estimated collecting efficiency of this system was estimated to be in excess of 95 percent for particles with diameters of about 100 to 500 microns in wind speeds less than about 5 miles per hour.[1]

The trays were set so that the top of the tray was about an inch or two above the level of surrounding grassy areas. Open grass-covered areas were always used as sites for locating the tray to minimize blow-in of soil or other particles from the immediate surrounding area. To allow for drainage of rainwater that would be collected during rain showers, a 3/4-inch hole was punched in the side wall of the tray for the attachment of a filtering system (see Reference 1 for details).

RESULTS

During the sampling periods from July 1964 through January 1965 of the second field phase of Operation Ceniza-Arena in Costa Rica, 22 sets of plate collector measurements were made. The exposure period for the sets ranged from 6 minutes to about 8 hours, but most of the exposures were for less than 1 hour. Except for two overnight exposures, the wind speeds and exposure times were measured as described. The weight measurements of the particles recovered from the plates and the exposure times for each set are summarized in Table 1. The plate deposit densities, corrected for background dust, and the average wind speed during the exposure period are given in Table 2. The average deposit density of the background dust was determined from the collections on the bottom or back side of the plates set at 0, 90, 120, 150, and 180 degrees; if the weight of the particles on the protected side of the plates set at 30 and 60 degrees was equal to or less than the largest background weight on the five other plates, it was also included in the average. The data from three sets for three different wind speeds are plotted in Figure 3. None of the curves can be represented or approximated by a sine function as might be described by Equation 2 with a constant value for the impaction coefficient.

The particles recovered from most of the plate collector sets were sieve-analyzed to determine the weight distributions. The samples recovered from each plate were sieve-analyzed separately when they were large enough to do so; the results for these plates are summarized in Table 3. The single plate data show that the distributions varied to some extent from one plate to another; however, no pattern of variation in the shape of the distribution curves with plate angle or with size of sample is readily apparent from the data.

The data for the gross weight distribution of the particles recovered from all the plates in all sets except Set No. 19 are summarized in Table 4; weight distribution curves of the particles recovered from the plates in several sample sets are shown in Figure 4. The values of d_{min}, d_{50}, and d_{max} given in Table 4 for the particles from all the sample sets were estimated from distribution curves that were constructed similarly to those shown in Figure 4. Even though the curves differ greatly from one another, the median diameter for the particles from all the sets is near 50 microns.

Table 1

SUMMARY OF PLATE COLLECTOR MEASUREMENTS

Set Number	Side of Plate	Plate Angle (degrees) 0	30	60	90	120	150	180	Exposure Time (min)
		m_o (gm/sq ft)[a]							
1	Top[b]	0.0344	0.0172	0.0183	0.2705	0.2705	0.1295	0.0504	71
	Bottom	0.0160	0.0344	0.2154	0.0115	0.0149	0.0115	0.0183	
2	Top	0.1008	0.0711	0.0745	0.7025	0.6567	0.3472	0.0848	60
	Bottom	0.0321	0.2063	0.4286	0.0172	0.0115	0.0092	0.0344	
3	Top	0.0483	0.0160	0.0160	0.0779	0.1377	0.0928	0.0493	72
	Bottom	0.0115	0.0160	0.0413	0.0080	0.0172	0.0138	0.0000	
4	Top	0.1788	0.1730	0.0745	0.1112	0.2097	0.2430	0.2223	25
	Bottom	0.0183	0.0206	0.0344	0.0160	0.0115	0.0080	0.0046	
5	Top	0.1490	0.0779	0.0504	0.1513	0.2418	0.2372	0.1536	30
	Bottom	0.0080	0.0206	0.0562	0.0138	0.0138	0.0115	0.0080	
6	Top	13.57	2.808	-	23.49	30.52	27.28	13.64	675
	Bottom	-	-	5.689	-	-	-	-	
7	Top	0.5042	0.3278	0.1329	0.0974	0.3278	0.4962	0.3713	10
	Bottom	0.0080	0.0138	0.0206	0.0103	0.0080	0.0126	0.0149	

a m_o is the measured weight divided by the plate area (0.08726 sq ft)

b Front face for plate angle of 90 degrees

Table 1 (continued)

Set Number	Side of Plate	Plate Angle (degrees) 0	30	60	90	120	150	180	Exposure Time (min)
		m_o (gm/sq ft)[a]							
8	Top[b]	0.2212	0.0699	0.0103	0.3610	0.5764	0.4848	0.1971	10
	Bottom	0.0069	0.0172	0.0951	0.0080	0.0103	0.0069	0.0092	
9	Top	0.1490	0.0367	0.0126	0.5272	0.6429	0.3427	0.1226	20
	Bottom	0.0057	0.0447	0.2097	0.0138	0.0126	0.0069	0.0115	
10	Top	0.0539	0.0057	0.0069	0.2808	0.3954	0.1536	0.0539	16
	Bottom	0.0046	0.0275	0.0963	0.0057	0.0080	0.0057	0.0069	
11	Top	0.0367	0.0264	0.0183	0.4114	0.3152	0.1112	0.0390	28
	Bottom	0.0069	0.0298	0.1604	0.0194	0.0046	0.0034	0.0011	
12	Top	0.1020	0.0504	0.0309	0.0619	0.1387	0.1341	0.0882	33
	Bottom	0.0034	0.0057	0.0126	0.0046	0.0034	0.0034	0.0069	
13	Top	0.0424	0.0241	0.0298	0.2086	0.1857	0.0951	0.0413	27
	Bottom	0.0069	0.0252	0.0837	0.0103	0.0103	0.0092	0.0069	
14	Top	0.0291	0.0166	0.0156	0.1302	0.1139	0.0536	0.0252	12
	Bottom	0.0077	0.0268	0.0898	0.0138	0.0154	0.0154	0.0092	
15	Top	0.0364	0.0260	0.0176	0.3179	0.2481	0.1060	0.0551	60
	Bottom	0.0264	0.0724	0.2032	0.0123	0.0253	0.0346	0.0235	

a m_o is the measured weight divided by the plate area (0.08726 sq ft)
b Front face for plate angle of 90 degrees

Table 1 (concluded)

Set Number	Side of Plate	Plate Angle (degrees) 0	30	60	90	120	150	180	Exposure Time (min)
		m_o (gm/sq ft)[a]							
16	Top[b]	0.0322	0.0096	0.0094	0.4325	0.3264	0.1117	0.0308	45
	Bottom	0.0102	0.0714	0.2642	0.0096	0.0155	0.0135	0.0165	
17	Top	1.1861	0.4446	0.2773	1.6468	2.4261	2.2049	1.1827	1,050
	Bottom	0.0046	0.0481	0.3633	0.0221	0.0138	0.0229	0.0241	
18	Top	0.5203	0.1799	0.1043	1.0474	1.3912	1.0807	0.4699	10
	Bottom	0.0115	0.0539	0.3919	0.0229	0.0183	0.0115	0.0126	
19	Top	0.1008	0.0481	0.0252	0.1306	0.2372	0.2064	0.1490	43
	Bottom	0.0080	0.0103	0.0355	0.0092	0.0092	0.0103	0.0080	
20	Top	0.1272	0.0252	0.0126	0.8733	0.9718	0.5673	0.1799	80
	Bottom	0.0172	0.1719	0.4859	0.0115	0.0080	0.0092	0.0160	
21	Top	0.0562	0.0275	0.0149	0.1639	0.1925	0.1341	0.0573	30
	Bottom	0.0115	0.0241	0.0848	0.0069	0.0160	0.0069	0.0115	
22	Top	0.7529	0.2441	0.0550	0.3358	1.1460	1.5551	0.7953	5
	Bottom	0.0172	0.0275	0.0596	0.0183	0.0126	0.0092	0.0115	

a m_o is the measured weight divided by the plate area (0.08726 sq ft)

b Front face for plate angle of 90 degrees

Table 2

SUMMARY OF CORRECTED PLATE COLLECTOR DATA

Set Number	Side of Plate	Plate Angle (degrees) 0	30	60	90	120	150	180	Background (gm/sq ft)	$\bar{v}_w^o$ (ft/sec)
		m (gm/sq ft)[a]								
1	Top[b]	0.0190	-	-	0.2551	0.2551	0.1141	0.0350	0.0154	6.0
	Bottom		0.0190	0.2000						
2	Top	0.0799	0.0502	0.0536	0.6816	0.6358	0.3263	0.0639	0.0209	7.3
	Bottom		0.1854	0.4077						
3	Top	0.0367	0.0044	-	0.0663	0.0961	0.0812	0.0177	0.0116	8.5
	Bottom		0.0044	0.0297						
4	Top	0.1671	0.1613	0.0628	0.0995	0.1980	0.2313	0.2106	0.0117	1.9
	Bottom		0.0089	0.0227						
5	Top	0.1380	0.0669	0.0394	0.1403	0.2308	0.2262	0.1426	0.0110	2.3
	Bottom		0.0096	0.0452						
6[c]	Top	13.56	2.797	-	23.48	30.51	27.27	13.63	0.011[d]	3.5[d]
	Bottom			5.678						
7	Top	0.4913	0.3149	0.1200	0.0845	0.3149	0.4833	0.3584	0.0129	2.0
	Bottom			0.0077						

a Inverse plate area is 11.46 ft^{-2}; m is the measured weight minus the background weight

b Front face for plate angle of 90 degrees

c Overnight exposure

d Estimated value

Table 2 (continued)

Set Number	Side of Plate	Plate Angle (degrees) 0	30	60	90	120	150	180	Background (gm/sq ft)	$\bar{v}_w^o$ (ft/sec)
		m (gm/sq ft)[a]								
8	Top[b]	0.2126	0.0613	-	0.3524	0.5678	0.4762	0.1885	0.0086	7.1
	Bottom		0.0086	0.0865						
9	Top	0.1385	0.0262	-	0.5167	0.6324	0.3322	0.1121	0.0105	9.7
	Bottom		0.0342	0.1992						
10	Top	0.0477	-	-	0.2746	0.3892	0.1474	0.0477	0.0062	13.2
	Bottom		0.0213	0.0901						
11	Top	0.0277	0.0174	-	0.4024	0.3062	0.1022	0.0300	0.0090	14.0
	Bottom		0.0208	0.1514						
12	Top	0.0974	0.0458	0.0263	0.0573	0.1341	0.1295	0.0836	0.0046	5.4
	Bottom			0.0080						
13	Top	0.0337	0.0154	0.0211	0.1999	0.1770	0.0864	0.0326	0.0087	11.9
	Bottom		0.0165	0.0750						
14	Top	0.0168	0.0043	0.0033	0.1179	0.1016	0.0413	0.0129	0.0123	9.2
	Bottom		0.0145	0.0775						
15	Top	0.0127	-	-	0.2942	0.2244	0.0823	0.0314	0.0237	14.4
	Bottom		0.0487	0.1795						

a Inverse plate area is 11.46 ft^{-2}; m is the measured weight minus the background weight

b Front face for plate angle of 90 degrees

Table 2 (concluded)

Set Number	Side of Plate	Plate Angle (degrees) 0	30	60	90	120	150	180	Background (gm/sq ft)	$\bar{v}_w^o$ (ft/sec)
					$\bar{m}$ (gm/sq ft)[a]					
16	Top[b]	0.0202	-	-	0.4205	0.3144	0.0997	0.0188	0.0120	14.8
	Bottom		0.0594	0.2522						
17[c]	Top	1.1686	0.4271	0.2598	1.6293	2.4086	2.1874	1.1652	0.0175	2.9[d]
	Bottom		0.0306	0.3458						
18	Top	0.5049	0.1645	0.0889	1.0320	1.3758	1.0653	0.4545	0.0154	11.2
	Bottom		0.0385	0.3765						
19	Top	0.0916	0.0389	0.0160	0.1214	0.2280	0.2372	0.1398	0.0092	4.7
	Bottom			0.0263						
20	Top	0.1148	0.0128	-	0.8609	0.9594	0.5549	0.1675	0.0124	11.3
	Bottom		0.1595	0.4735						
21	Top	0.0449	0.0162	-	0.1526	0.1812	0.1228	0.0460	0.0113	7.6
	Bottom		0.0128	0.0735						
22	Top	0.7391	0.2303	0.0412	0.3220	1.1322	1.5413	0.7815	0.0138	5.8[d]
	Bottom		0.0137	0.0458						

a Inverse plate area is 11.46 ft^{-2}; m is the measured weight minus the background weight

b Front face for plate angle of 90 degrees

c Overnight exposure

d Estimated value

Figure 3

VARIATION OF PLATE COLLECTOR DEPOSITS WITH PLATE ANGLE

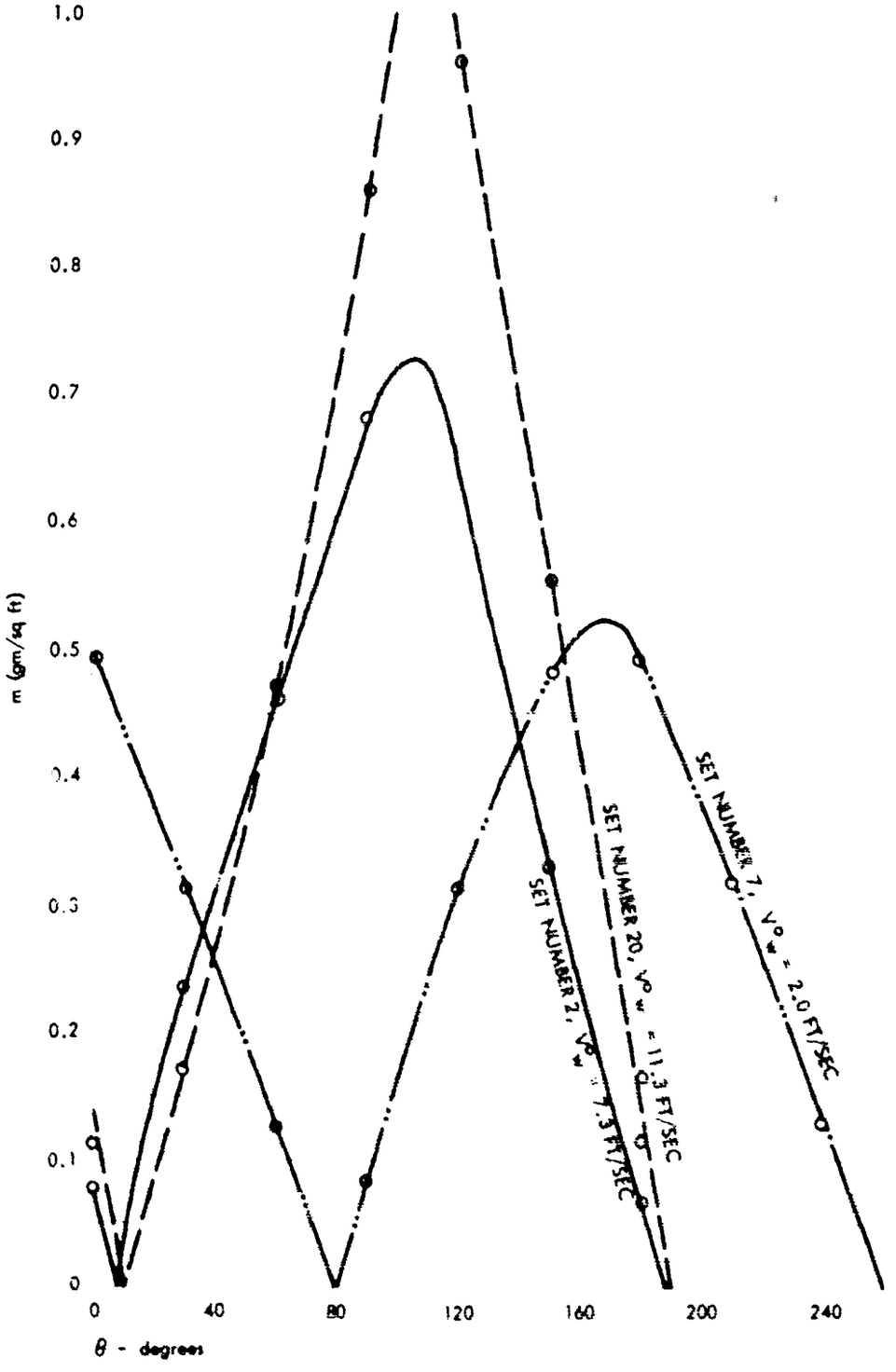

Table 3

WEIGHT DISTRIBUTION OF PARTICLES RECOVERED
FROM THE PLATE COLLECTOR (SINGLE PLATE)

Set Number	Plate Angle (degrees)	Accumulated Weight Percentage (particle diameter in microns) 46	105	250	>250	d_{50}[a] (microns)	w_c (mg)
1	0,180	7.69	69.2	89.7	100	85	10.4
	30	Nil	83.3	100	-	(90)	4.5
	60	29.3	87.8	100	-	60	20.4
	90	19.0	84.8	98.4	100	67	24.6
	120	10.5	79.0	100	-	76	24.9
	150	15.5	81.7	97.2	100	71	12.3
2	0,180	44.3	85.7	97.9	100	51	22.0
	30	35.8	97.4	100	-	53	24.2
	60	42.2	97.0	100	-	50	43.9
	90	42.4	95.2	100	-	50	62.8
	120	39.8	96.0	100	-	51	58.3
	150	53.6	97.9	100	-	44	31.1
4	0,180	28.6	98.3	100	-	55	35.0
	30	26.8	95.1	100	-	58	15.1
	60	22.4	97.0	100	-	58	9.5
	90	21.3	94.7	100	-	60	9.7
	120	24.8	99.4	100	-	55	18.3
	150	25.4	98.2	100	-	56	21.2
5	0,180	37.7	99.1	100	-	50	26.4
	30	32.6	95.6	100	-	55	6.8
	60	37.1	98.6	100	-	51	9.3
	90	32.4	100.0	-	-	(50)	13.2
	120	34.5	100.0	-	-	(49)	21.1
	150	35.1	98.8	100	-	52	20.7
6	0,180	39.4	82.3	100	-	56	2,374.0
	30	42.9	84.5	100	-	52	245.0

a Assuming a log normal weight distribution for diameters between about 30 and 105 microns; values in parentheses are estimated values

Table 3 (continued)

Set Number	Plate Angle (degrees)	Accumulated Weight Percentage (particle diameter in microns) 46	105	250	>250	d_{50}[a] (microns)	w_c (mg)
6	60	52.4	94.0	100	-	44	496.4
	90	37.2	83.4	100	-	57	2,049.8
	120	35.2	77.0	100	-	62	2,662.8
	150	33.7	79.5	100	-	61	2,380.4
7	0,180	43.7	92.3	100	-	50	76.4
	30	42.3	91.9	100	-	51	28.6
	60	34.7	91.6	100	-	55	13.4
	90	43.3	96.7	100	-	50	8.5
	120	40.8	98.5	100	-	50	23.6
	150	41.6	90.3	100	-	52	43.3
8	0,180	41.0	80.4	100	-	55	36.5
	30	37.5	95.8	100	-	51	7.6
	60	50.0	98.0	100	-	46	8.3
	90	55.9	89.5	100	-	41	31.5
	120	46.8	81.4	100	-	49	50.3
	150	48.6	80.9	100	-	48	42.3
9	0,180	60.4	89.8	100	-	37	23.7
	30	46.0	96.0	100	-	48	7.1
	60	61.4	94.3	100	-	41	18.3
	90	59.7	90.6	100	-	38	46.0
	120	55.7	88.4	100	-	41	56.1
	150	60.6	88.3	100	-	36	29.9
10	0,180	31.8	77.3	100	-	63	9.4
	30	44.4	88.9	100	-	50	2.4
	60	36.9	80.0	100	-	58	8.4
	90	61.9	78.8	100	-	28	24.5
	120	38.0	75.1	100	-	60	34.5
	150	35.6	74.3	100	-	62	13.4

a Assuming a log normal weight distribution for diameters between about 30 and 105 microns

Table 3 (continued)

Set Number	Plate Angle (degrees)	Accumulated Weight Percentage (particle diameter in microns) 46	105	250	>250	d_{50}[a] (microns)	w_c (mg)
11	0,180	27.9	76.7	100	-	66	6.6
	30	29.4	94.1	100	-	57	4.9
	60	40.7	89.8	100	-	52	14.0
	90	41.5	83.8	100	-	54	35.9
	120	39.2	81.4	100	-	56	27.5
	180	40.0	83.8	100	-	55	9.7
12	0,180	21.1	95.2	100	-	60	16.6
	30	9.68	90.3	100	-	70	4.4
	60	21.0	95.2	100	-	60	2.7
	90	24.7	97.3	100	-	57	5.4
	120	8.33	95.8	100	-	66	12.1
	150	32.9	97.3	100	-	54	11.7
13	0,180	30.1	84.9	98.6	100	60	7.3
	30	13.6	81.8	100	-	72	4.3
	60	34.2	89.6	99.3	100	54	7.3
	90	41.2	87.8	100	-	53	18.2
	120	33.3	86.0	100	-	58	16.2
	150	36.2	87.2	100	-	56	8.3

Set Number	Plate Angle (degrees)	Accumulated Weight Percentage (particle diameter in microns) 44	88	175	295	>295	d_{50}[a] (microns)	w_c (mg)
14	60	18.5	93.8	99.9	100	-	57	9.2
	90	30.8	100	-	-	-	(48)	11.4
	120	17.1	92.7	97.6	100	-	58	9.9
15	60	39.6	89.2	100	-	-	50	19.3
	90	27.5	84.1	100	-	-	57	28.8
	120	42.2	85.3	99.5	100	-	49	26.8

---

a Assuming a log normal weight distribution for diameters between about 30 and 105 microns; values in parentheses are estimated values

Table 3 (concluded)

Set Number	Plate Angle (degrees)	Accumulated Weight Percentage (particle diameter in microns) 44	88	175	295	>295	d_{50}[a] (microns)	w_c (mg)
16	60	38.7	83.1	90.9	94.6	100	51	23.9
17	0,180	47.1	91.5	98.5	99.3	100	46	209.2
	30	36.9	84.7	95.2	97.0	100	52	43.0
	60	44.4	93.4	96.8	98.5	100	47	55.9
	90	44.2	93.5	99.1	99.3	100	47	146.5
	120	44.8	90.4	99.1	99.5	100	47	212.9
	150	40.6	79.0	87.6	99.4	100	52	194.4
18	0,180	28.6	73.8	96.3	97.5	100	61	88.5
	30	23.8	74.6	100	-	-	63	20.4
	60	31.5	81.6	94.5	96.6	100	56	43.3
	90	30.3	90.7	98.1	98.7	100	53	93.4
	120	27.9	78.3	99.3	99.8	100	59	123.0
	150	28.9	73.9	98.0	98.9	100	61	95.3
22	0	36.0	60.0	87.3	98.6	100	67	65.7
	150	39.6	60.3	84.9	99.0	100	63	135.7

a Assuming a log normal weight distribution for diameters between about 30 and 105 microns

Table 4

WEIGHT DISTRIBUTION OF PARTICLES RECOVERED FROM THE PLATE COLLECTOR (ALL PLATES)

Set Number	Accumulated Weight Percentage (particle diameter in microns)				d_{min} (microns)	d_{50} (microns)	d_{max} (microns)	$\bar{v}_f$ [a] (ft/sec)
	46	105	250	>250				
1	16.3	81.9	98.4	100.0	32	68	380	1.24
2	42.8	95.5	99.84	100.0	30	49	320	0.73
4	26.0	97.7	100.0	100.0	41	50	170	0.76
5	35.4	99.09	100.0	100.0	37	50	210	0.76
6	37.2	81.1	100.0	100.0	33	52	240	0.81
7	42.1	92.8	100.0	100.0	36	48	200	0.71
8	47.7	83.6	100.0	100.0	31	47	240	0.68
9	58.4	89.9	100.0	100.0	30	43	240	0.58
10	44.2	76.9	98.7	100.0	29	49	280	0.73
11	39.3	84.0	100.0	100.0	33	50	240	0.76
12	20.2	95.6	100.0	100.0	32	60	135	1.02
13	34.4	86.7	99.75	100.0	34	51	260	0.78

a Applicable to d_{50} for a spherical particle in air at an altitude of 6,000 to 10,000 ft msl

Table 4 (concluded)

Set Number	Accumulated Weight Percentage (particle diameter in microns)					d_{min} (microns)	d_{50} (microns)	d_{max} (microns)	$\bar{v}_f$ [a] (ft/sec)
	44	88	175	295	>295				
3	45.2	62.5	71.8	89.1	100.0	7	52	430	0.81
14	26.8	93.7	99.01	100.0	100.0	35	50	290	0.76
15	43.9	86.6	99.88	100.0	100.0	10	48	185	0.71
16	36.5	89.1	97.9	98.7	100.0	21	50	600	0.76
17	43.6	88.0	95.6	99.19	100.0	18	47	350	0.68
18	28.9	78.9	97.8	98.6	100.0	16	58	700	0.97
20	48.3	89.4	98.9	100.0	100.0	32	45	230	0.63
21	22.8	72.9	99.20	100.0	100.0	29	62	190	1.05
22	38.8	64.2	88.5	99.42	100.0	4	60	320	1.02

[a] Applicable to d_{50} for a spherical particle in air at an altitude of 6,000 to 10,000 ft msl

Figure 4

WEIGHT DISTRIBUTION CURVES FOR SEVERAL PLATE COLLECTOR SAMPLES

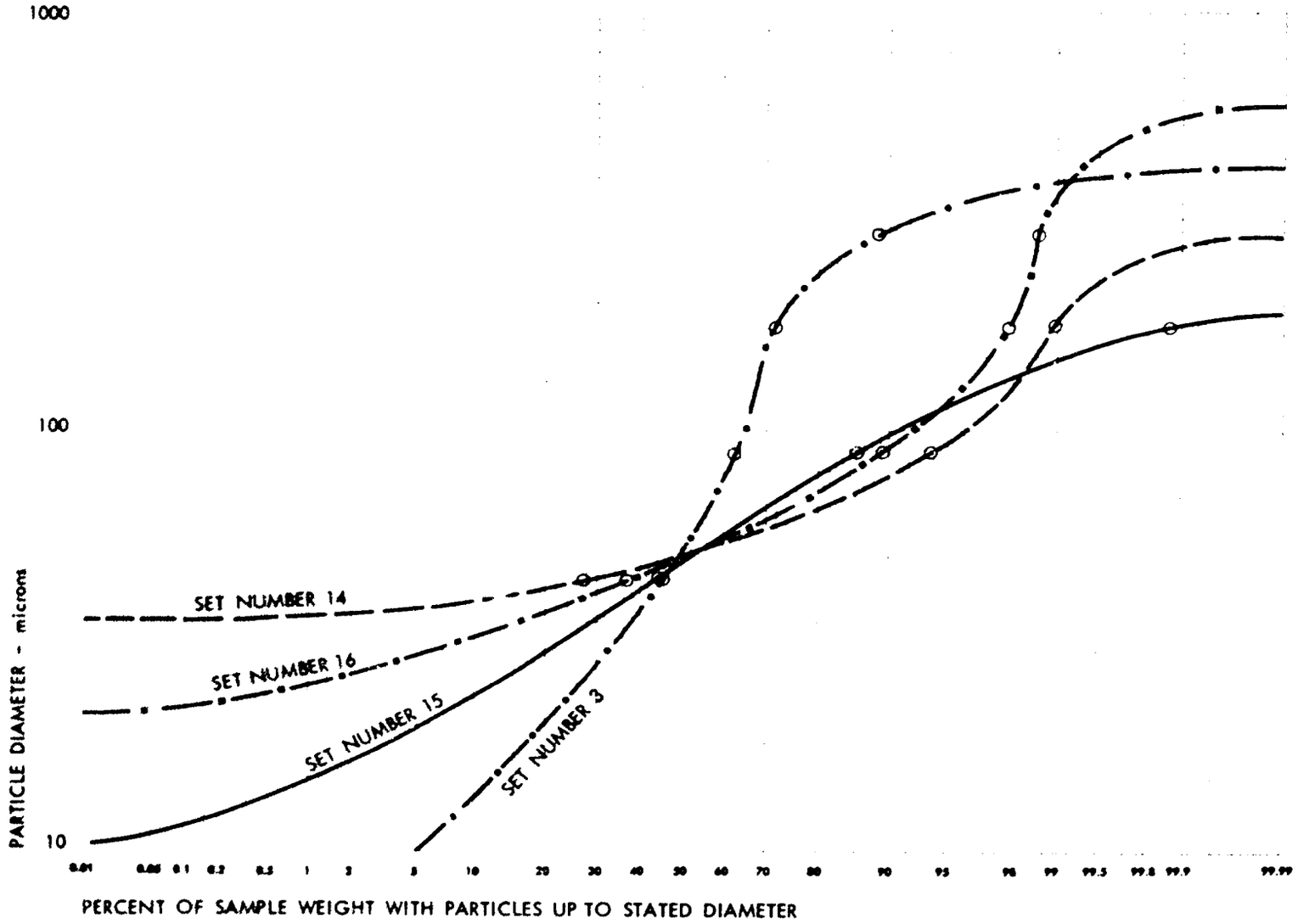

The shape of most of the weight distribution curves, as shown by those for Set Nos. 3, 14, and 16, indicates the presence of two distributions in the sieved sample. The second distribution was presumably formed during the sieve analysis by the breakage of agglomerated particles into their basic soil or mineral grain sizes. As a first approximation, the curves indicate that, for Set No. 3, about 80 percent of the weight was in the form of agglomerated particles and, for Set Nos. 14 and 16, about 99 percent of the weight arrived on the plates in the form of agglomerated particles.

Collections of ceniza-arena at ground level by tray were made simultaneously with the exposure of the plate collector for only a few sets. Estimates of the ground level collections during other exposures were made from the deposit records of a modified dew balance (see References 1 and 2). The data for the ground level collections by tray and those from the modified dew balance records for each plate collector exposure are summarized in Table 5. The mass median particle diameters from a sieve-analysis of the particles collected on the trays (some with overlapping exposure periods) and the average wind speed for the total tray deposit (see Reference 2) are also given in Table 5.

Table 5

SUMMARY OF GROUND LEVEL CENIZA-ARENA DEPOSIT DATA[a]

Set Number	Tray Number	m_g (gm/sq ft)	d_{50} (microns)	$\bar{v}_w^o$ (ft/sec)
1	14113	0.1317	59	6.0
2	14176	(0.42)[b]	57	-
3	14209	0.1038	225	8.5
4	14264	0.1508	47	1.9
5	14265	0.1590	52	9.2
6	14271	19.112	60	2.5
7	14290	(0.124)	54	2.5
8	14335	(0.62)	66	4.1
9	14335	(0.42)	66	4.1
10	14352	(0.30)	63	13.6
11	14352	(0.40)	63	13.6
12	14390	(0.10)	57	7.0
13	14390	(0.13)	57	7.0
14	14573	(0.12)	49	13.2
15	14591	(0.14)	62	16.7
16	14591	(0.14)	62	16.7
17	13502	1.6821	50	-
18	13502	0.8968	70	11.2
19	13509	0.2245	87	4.7
20	06475	0.7982	78	6.6
21	06504	0.3512	86	7.3
22	15036	0.7724	60	5.8

---

a Locations and sampling dates and data on d_{50} and $\bar{v}_w^o$ are given in Reference 2.

b Values in parentheses are estimated from dew balance records (as described in Reference 2).

DATA ANALYSIS

In correlating and analyzing the plate collector data, another major assumption was that the impaction behavior of the particles varied with the ratio, $\bar{v}_w^o/\bar{v}_f^o$ (or cot $\bar{\varphi}$), within the limits of accuracy of the data. This assumption implies the same degree of impaction for the larger particles that impact under the higher wind speed conditions as for the smaller particles that impact under lower wind speeds.

The derived values of the constants for Equation 7 (class one geometry) are summarized in Table 6. The applicable plate angles for this geometry from Table 2 are 90, 120, 150, and 0 or 180 degrees. Since Equation 7 contains four unknown parameters, the data for the four plates permitted a single solution for the value of each parameter; the single duplicate solution for each set occurs because of the two horizontal plates. Thus variations in the parameter values because of experimental fluctuations or error in the data can only be inferred from the duplicate solutions for the two horizontal plates.

The values of $\theta - 90$ are plotted as a function of $\bar{\varphi}$ in Figure 5; the points for the paired solutions for each set are connected by lines to illustrate the degree of variance in these two parameters that resulted from the experimental error in the m values for the two horizontal plates. In 14 of the sets, the data of Figure 5 indicate that θ_o is about 90 degrees larger than $\bar{\varphi}$. In most of the other sets where the points fall below the line for θ_o equal to $\bar{\varphi} + 90$, the wind speeds usually were high. If the value of $\bar{\varphi}$ actually was 10 degrees or smaller, slight fluctuations in the wind speed during deposition combined with the distribution in diameters of the particle would result in a higher value of m for the horizontal plates than would occur if the wind speed were constant and all the particles had the same diameter. Under these conditions, the derived value of $\bar{\varphi}$ would always be larger than the true value.

The dependence of values of γ on cot $\bar{\varphi}$ and cot $(\theta_o - 90)$, as derived from Equation 7, is shown in Figure 6. The data show that the value of γ has no significant dependence on cot $\bar{\varphi}$ but that its value increases as the value of cot $(\theta_o - 90)$ increases.

The derived values of $\bar{\varphi}$ and γ by use of Equation 8 (class one geometry), in which θ_o is set equal to $\bar{\varphi} + 90$, are summarized in Table 7.

Table 6

SUMMARY OF DERIVED CONSTANTS FOR EQUATION 7, CLASS ONE GEOMETRY[a]

Set Number	$\bar{\varphi}$ (degrees)	θ_o (degrees)	θ_o-90 (degrees)	0.434γ	$\eta^o m_a$ (gm/sq ft)	$\bar{v}^o_w/\bar{v}^o_f$	$\bar{v}^o_f$ (ft/sec)
1	9°50'	107°40'	18°40'	0.2248	0.2848	5.77	1.04
	24°46'	100°56'	10°56'	0.2837	0.2944	2.17	2.77
2	12°39'	101°07'	11°07'	0.1522	0.7168	4.46	1.64
	9°15'	103°32'	13°32'	0.1347	0.7145	6.14	1.19
3	30°21'	132°06'	42°06'	0.1200	0.1200	1.71	4.98
	31°43'	130°34'	40°34'	0.1172	0.09790	1.62	5.25
4	57°13'	140°34'	50°34'	0.08817	0.2342	0.644	2.95
	67°38'	175°14'	85°14'	-0.03026	0.2275	0.411	4.62
5	46°28'	130°28'	40°28'	0.09335	0.2441	0.950	2.42
	48°29'	127°18'	37°18'	0.08635	0.2449	0.885	2.60
6	27°02'	147°21'	57°21'	0.06437	32.52	1.96	1.79
	27°16'	147°01'	57°01'	0.06345	32.44	1.94	1.80
7	76°57'	158°16'	68°16'	0.03808	0.5128	0.195	10.2
	72°23'	145°09'	55°09'	0.1867	0.4979	0.318	6.30
8	35°47'	128°12'	38°12'	0.1640	0.5797	1.39	5.12
	29°24'	133°10'	43°24'	0.1767	0.5920	1.78	4.00

a The parameter values in the first line of each set are derived from the m values of Table 2 for plate angles of 0, 90, 120, and 150 degrees; those in the second line are derived from the m values for plate angles of 90, 120, 150, and 180 degrees.

Table 6 (concluded)

Set Number	$\bar{\varphi}$ (degrees)	θ_o (degrees)	θ_o-90 (degrees)	0.434γ	$\eta^o m_a$ (gm sq/ft)	$\bar{v}^o_w/\bar{v}^o_f$	$\bar{v}^o_f$ (ft/sec)
9	43°13'	101°18'	11°18'	0.2950	0.7470	1.06	9.12
	31°04'	107°12'	17°18'	0.2688	0.6722	1.66	5.84
10	56°20'	101°48'	11°48'	0.5110	0.5465	0.666	19.8
11	20°53'	93°50'	3°50'	0.3752	0.4341	2.62	5.34
	23°47'	93°16'	3°16'	0.3884	0.4423	2.27	6.17
12	72°42'	100°24'	10°24'	0.1478	0.1970	0.312	17.3
	67°56'	113°16'	23°16'	0.1658	0.1718	0.405	13.3
13	26°05'	92°28'	2°28'	0.2324	0.2230	2.04	5.82
	24°41'	92°55'	2°55'	0.2262	0.2206	2.18	5.47
14	36°05'	92°12'	2°12'	0.3554	0.1462	1.37	6.71
	23°23'	95°30'	5°30'	0.3040	0.1301	2.31	3.98
15	8°04'	95°02'	5°02'	0.2622	0.3000	7.06	2.04
	31°32'	90°16'	0°16'	0.3798	0.3452	1.63	8.83
16	14°01'	95°10'	5°10'	0.3638	0.4394	4.01	3.69
	12°37'	95°27'	5°27'	0.3562	0.4373	4.47	3.31
17	36°34'	132°46'	42°46'	0.09386	2.476	1.35	2.15
	36°24'	133°00'	43°00'	0.09450	2.478	1.36	2.14
18	33°01'	118°06'	28°06'	0.1108	1.378	1.54	7.28
	27°45'	124°57'	34°57'	0.1124	1.382	1.90	5.89
19	25°27'	147°48'	57°48'	0.2315	0.2885	2.10	2.24
	48°48'	135°22'	45°22'	0.1331	0.2514	0.875	5.37
20	10°48'	118°24'	28°24'	0.1423	1.016	5.24	2.16
	18°57'	110°28'	20°28'	0.1634	0.9980	2.91	3.88
21	22°09'	116°26'	26°26'	0.1168	0.1833	2.46	3.09
	23°03'	115°21'	25°21'	0.1198	0.1840	2.35	3.23
22	57°33'	141°58'	51°58'	0.3413	1.591	0.636	9.12
	60°24'	141°20'	51°20'	0.3184	1.593	0 568	10.2

Figure 5

VARIATION OF (θ_o-90) WITH $\bar{\phi}$, EQUATION 7

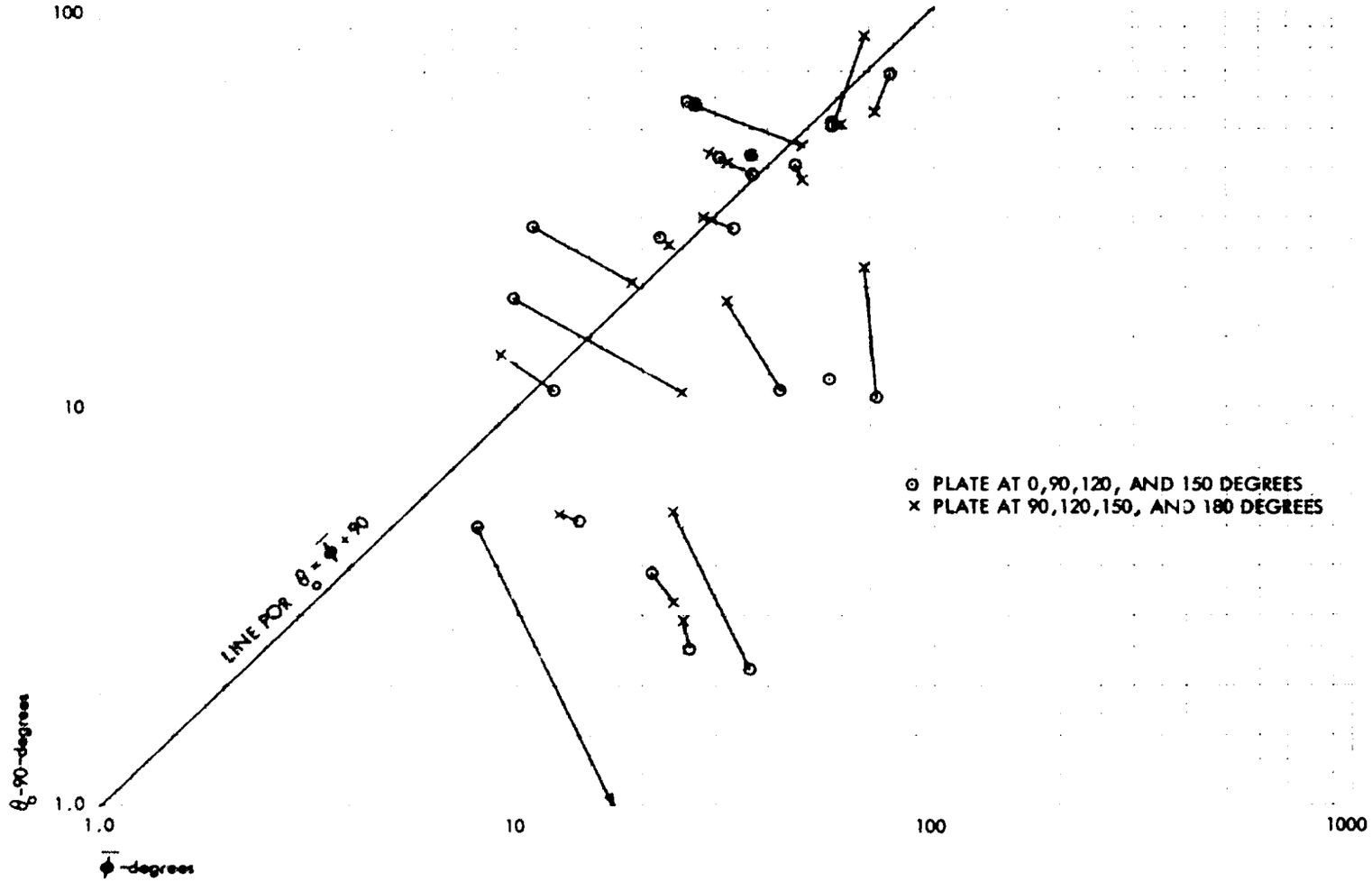

Figure 6

VARIATION OF γ WITH COT $\bar{\phi}$ AND COT (θ_o-90), EQUATION 7

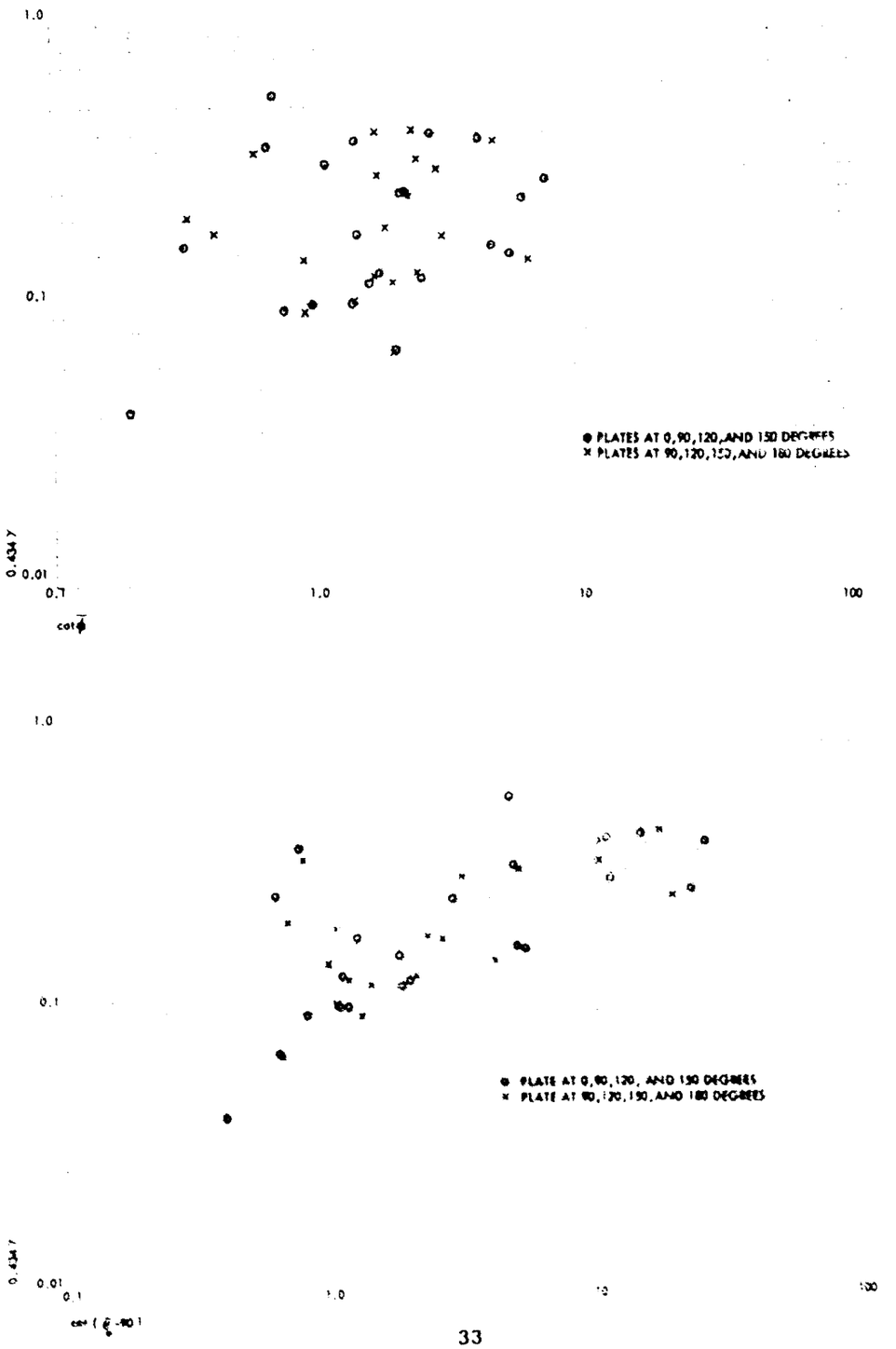

Table 7

SUMMARY OF DERIVED CONSTANTS FOR EQUATION 8, CLASS ONE GEOMETRY

Set Number	A[a]		B[a]		C[a]		D[a]	
	$\bar{\varphi}$	0.434γ	$\bar{\varphi}$	0.434γ	$\bar{\varphi}$	0.434γ	$\bar{\varphi}$	0.434γ
1	15°00'	0.2471	15°00'	0.3210	6°45'	0.1034	7°52'	0.1774
	15°00'	0.2471	15°00'	0.3210	NS[b]	NS[b]	NS[b]	NS[b]
2	11°41'	0.1473	11°28'	0.1292	NS	NS	13°14'	0.1613
	11°41'	0.1473	12°18'	0.2013	8°10'	0.0963	8°40'	0.1219
3	35°42'	0.1102	34°21'	0.1268	34°57'	0.1482	37°40'	0.1710
	35°42'	0.1102	34°43'	0.1222	35°08'	0.1370	37°13'	0.1540
4	53°23'	0.1147	55°02'	0.1012	55°21'	0.0914	54°40'	0.0842
5	43°52'	0.1027	44°40'	0.0962	44°40'	0.0887	43°44'	0.0813
	43°52'	0.1027	45°21'	0.0908	45°20'	0.0778	43°37'	0.0640
6	35°53'	0.0369	33°03'	0.0639	34°23'	0.1017	39°36'	0.1441
	35°53'	0.0369	33°07'	0.0632	34°25'	0.0993	39°32'	0.1412
7	79°27'	0.0263	79°54'	0.0180	75°59'	0.0918	76°17'	0.0487
	56°16'	0.3662	62°01'	0.3152	64°52'	0.2370	62°49'	0.1908
8	37°04'	0.1615	36°47'	0.1651	36°53'	0.1698	37°28'	0.1748
	37°04'	0.1615	35°20'	0.1848	36°01'	0.2158	38°51'	0.2417
9	21°56'	0.2496	24°00'	0.1647	NS	NS	NS	NS
	21°56'	0.2496	22°50'	0.2060	NS	NS	NS	NS
10	22°34'	0.4612	24°51'	0.3292	NS	NS	NS	NS
11	6°43'	0.2983	NS[b]	NS[b]	NS	NS	NS	NS
12	43°56'	0.2832	53°12'	0.1848	56°18'	0.0709	NS	NS
	43°56'	0.2832	50°24'	0.2180	51°54'	0.1280	42°19'	0.0434
13	9°16'	0.1498	NS	NS	NS	NS	NS	NS
	9°16'	0.1498	NS	NS	NS	NS	NS	NS
14	9°45'	0.2382	NS	NS	NS	NS	NS	NS
	9°45'	0.2382	NS	NS	NS	NS	NS	NS

Table 7 (concluded)

Set Number	A[a]		B[a]		C[a]		D[a]	
	$\bar{\varphi}$	0.434γ	$\bar{\varphi}$	0.434γ	$\bar{\varphi}$	0.434γ	$\bar{\varphi}$	0.434γ
15	5°36'	0.2460	NS[b]	NS[b]	NS[b]	NS[b]	8°59'	0.2780
	5°36'	0.2460	NS	NS	NS	NS	NS[b]	NS[b]
16	6°37'	0.3200	NS	NS	NS	NS	NS	NS
	6°37'	0.3200	NS	NS	NS	NS	NS	NS
17	39°08'	0.0873	38°23'	0.0942	38°33'	0.1027	39°45'	0.1122
	39°08'	0.0873	38°19'	0.0949	38°31'	0.1038	39°47'	0.1138
18	30°53'	0.1112	31°22'	0.1044	30°57'	0.0939	NS	NS
	30°53'	0.1112	30°10'	0.1220	30°49'	0.1385	33°22'	0.1601
19	46°57'	0.1416	NS	NS	NS	NS	46°06'	0.3155
	46°57'	0.1416	47°28'	0.1371	47°31'	0.1316	47°01'	0.1267
20	19°48'	0.1658	18°38'	0.2531	24°07'	0.1953	8°11'[c]	0.0640[c]
	19°48'	0.1658	19°42'	0.1713	20°25'	0.1862	17°06'[d]	0.1373[d]
21	24°06'	0.1195	23°44'	0.1290	24°39'	0.1482	28°39'[e]	0.1864[e]
	24°06'	0.1195	23°55'	0.1247	24°23'	0.1345	27°21'[f]	0.1640[f]
22	52°54'	0.3736	53°57'	0.3630	54°11'	0.3470	53°34'	0.3343
	52°54'	0.3736	54°41'	0.3557	55°08'	0.3292	54°07'	0.3091

---

a A for plates at 90, 120, and 150 degrees; B for plates at 90, 120, and 0 or 180 degrees; C for plates at 90, 150, and 0 or 180 degrees; D for plates at 120, 150, and 0 or 180 degrees

b NS indicates no solution for $\bar{\varphi}$ and γ

c Alternate solution: $\bar{\varphi} = 33°14'$; $\gamma = 0.4753$

d Alternate solution: $\bar{\varphi} = 24°49'$; $\gamma = 0.2346$

e Alternate solution: $\bar{\varphi} = 18°01'$; $\gamma = 0.0614$

f Alternate solution: $\bar{\varphi} = 19°29'$; $\gamma = 0.0738$

Equation 7 contains only three unknown parameters so that for each set of data 4 to 8 paired values of $\bar{\varphi}$ and γ are possible; in some cases two solutions occur for combinations of three data points. The summary of Table 7 shows that for the sets where $\bar{\varphi}$ is small (high wind speed, small particle diameters), no solutions occur for the combinations that include the m values for the horizontal plates.

There is one additional estimate of the value of $\bar{\varphi}$ for each set: the data for the plates of class three geometry (particles deposited on the bottom face of the plates at 30 and 60 degrees and the front face of the plates at 90 degrees). For these plates, it was assumed that the impaction coefficient is proportional to $\sin(\theta - \bar{\varphi})$ so that

$$m = \frac{\eta^{o}m_{a}}{2}\left[1 - \cos 2(\theta - \bar{\varphi})\right] \qquad (10)$$

The values of $\eta^{o}m_{a}$ and $\bar{\varphi}$ for Equation 10 as derived from the m values for the class three geometry deposits are summarized in Table 8. For the cases in which Equation 10 gave two solutions for $\bar{\varphi}$ and $\eta^{o}m_{a}$, both sets of values are listed; one solution, however, gave $\bar{\varphi}$ values larger than the lowest value of θ used in Equation 10.

Using the parameter values of Tables 6, 7, and 8, the relationships shown in Figures 5 and 6, and the above discussion regarding the latter, it is concluded that the impaction data for the class one geometry are represented better by Equation 8 than by Equation 7. The data of Table 7 were therefore further analyzed for consistency with respect to the values of γ and their dependence on cot $\bar{\varphi}$ (or $\bar{v}^{o}_{w}/\bar{v}^{o}_{f}$). For most sets, this analysis resulted in the selection of one set of solutions for $\bar{\varphi}$, γ, and $\eta^{o}m_{a}$ from those listed; in a few cases, average values of the constants were taken. The selected values of the parameters are given in Table 9; the values of γ are plotted as a function of cot $\bar{\varphi}$ in Figure 7. The line drawn through the points is given by the equation

$$\gamma = 0.230\ (\bar{v}^{o}_{w}/\bar{v}^{o}_{f})^{1/2} = 0.230\ \cot^{1/2}\bar{\varphi} \qquad (11)$$

In deriving a relationship for representing the dependence of the impaction coefficient on the θ and $\bar{\varphi}$ for the class two geometry, the derived values of $\eta^{o}m_{a}$ and $\bar{\varphi}$ given in Table 9 were used to calculate the values of η/η^{o} for the plate angles of 30 and 60 degrees; in this form, the values of η for this geometry are relative to η^{o} for the class one geometry plates. The value of η for the plates at 0 and 180 degrees, from Equation 8, is given by

Table 8

SUMMARY OF DERIVED CONSTANTS FOR EQUATION 10, CLASS THREE GEOMETRY

Set Number	A^a		B^a		C^a	
	$\bar{\varphi}$	$\eta^o{}_{m_a}$ (gm/sq ft)	$\bar{\varphi}$	$\eta^o{}_{m_a}$ (gm/sq ft)	$\bar{\varphi}$	$\eta^o{}_{m_a}$ (gm/sq ft)
1	14°42'	0.2727	NS[b]	NS[b]	18°08'	0.4492
2	NS[b] (49°43')[c]	NS[b] (0.6862)[c]	(74°04')[c] NS	(3.385)[c] NS	(36°56')[c] (42°01')	(1.303)[c] (4.277)
3	NS (41°11')	NS (0.1170)	10°30' NS	0.7050 NS	NS[b] (38°13')	NS[b] (0.2157)
4	15°39' (42°42')	0.0715 (0.1842)	21°29' 37°50'	0.0766 0.1595	13°54' (41°29')	0.0572 (0.2251)
5	(41°20') 15°23'	(0.2488) 0.1090	30°50' NS	0.1903 NS	(39°21') 9°04'	(0.3634) 0.0750
6	-	-	36°49'	36.63	-	-
7	-	-	48°27'	0.1921	-	-
8	(36°56') NS	(0.6277) NS	36°33' NS	0.6151 NS	(37°04') 17°46'	(0.5697) 0.1915
9	15°39' (41°10')	0.5572 (0.9118)	26°07' NS	0.6409 NS	12°05' (38°40')	0.3616 (1.505)
10	(41°57') 14°21'	(0.4964) 0.2926	30°23' NS	0.3690 NS	(39°42') NS	(0.7486) NS
11	17°29' (40°02')	0.4423 (0.6864)	26°48' NS	0.5051 NS	14°44' (37°59')	0.2988 (1.077)
12	-	-	44°34'	0.1129	-	-
13	13°48' (42°16')	0.2120 (0.3650)	26°53' NS	0.2513 NS	NS (39°28')	NS (0.6096)

Table 8 (concluded)

Set Number	A[a] $\bar{\varphi}$	A[a] $\eta^{\circ}_{m_a}$ (gm/sq ft)	B[a] $\bar{\varphi}$	B[a] $\eta^{\circ}_{m_a}$ (gm/sq ft)	C[a] $\bar{\varphi}$	C[a] $\eta^{\circ}_{m_a}$ (gm/sq ft)
14	NS[b]	NS[b]	6°10'	0.1193	10°55'	0.1357
	(44°34')[c]	(0.2323)[c]	(73°13')[c]	(1.414)[c]	(38°55')[c]	(0.5989)[c]
15	(46°19')	(0.6167)	(73°07')	(3.488)	(40°11')	(1.562)
16	8°10'	0.4292	10°23'	0.4341	NS[b]	NS[b]
	(45°19')	(0.8504)	(73°03')	(4.947)	(39°09')	(1.991)
17	(36°20')	(2.510)	39°02'	2.700	(36°45')	(2.219)
18	(38°40')	(1.693)	27°39'	1.315	(37°08')	(2.493)
	19°31'	1.162	71°13'	(9.954)	17°32'	0.8259
19	-	-	38°42'	0.1993	-	-
	-	-	(69°25')	(9.822)	-	-
20	NS	NS	13°58'	0.9142	NS	NS
	(47°03')	(1.854)	(72°43')	(9.754)	(40°56')	(4.437)
21	NS	NS	18°59'	0.1701	NS	NS
	(42°21')	(0.2785)	(72°14')	(1.634)	(38°43')	(0.5578)
22	(39°12')	(0.5362)	44°21'	0.6297	(40°31')	(0.4117)

a A for plates at 30 and 90 degrees; B for plates at 60 and 90 degrees; C for plates at 30 and 60 degrees

b NS indicates that no solution of Equation 10 was possible.

c Values in parentheses are for solutions of $\bar{\varphi}$ greater than the lowest of the two θ values used in the equations.

Table 9

SUMMARY OF SELECTED VALUES OF DERIVED CONSTANTS FOR EQUATION 8, CLASS ONE GEOMETRY

Set Number	$\bar{\Phi}$	$\bar{v}^o_w/\bar{v}^o_f$	$0.434\bar{\gamma}$	$\eta^o m_a$ (gm/sq ft)	$\bar{v}^c_f$ (ft/sec)
1	10°29'	5.40	0.1909	0.3640	1.11
2	12°18'	4.59	0.2013	0.7272	1.59
3	34°43'	1.44	0.1222	0.09681	5.90
4	54°40'	0.709	0.0842	0.2331	2.68
5	43°52'	1.04	0.1027	0.2443	2.21
6	39°34'	1.21	0.1426	31.52	2.89
7	76°17'	0.244	0.0487	0.5123	8.20
8	37°04'	1.32	0.1615	0.5787	5.38
9	24°00'	2.25	0.1647	0.6412	4.31
10	24°51'	2.16	0.3292	0.3955	6.11
11	6°43'	8.49	0.2978	0.4128	1.65
12	56°18'	0.667	0.0709	0.1267	8.10
13	9°16'	6.13	0.1498	0.2063	1.94
14	9°45'	5.82	0.2382	0.1235	1.58
15	7°06'	8.01	0.2615	0.2959	1.80
16	6°37'	8.62	0.3200	0.4319	1.72
17	39°46'	1.20	0.1130	2.482	2.41
18	30°29'	1.70	0.1300	1.396	6.59
19	47°01'	0.932	0 1267	0.2507	5.04[a]
20	19°48'	2.78	0 1658	0.9987	4.06[a]
21	24°39'	2.18	0.1482	0.1892	3.49[a]
22	53°56'	0.728	0.3475	1.604	7.97[a]

a Value not corrected for vertical velocity component of the wind speed

Figure 7

VARIATION OF SELECTED VALUES OF γ WITH COT $\bar{\phi}$, CLASS ONE GEOMETRY

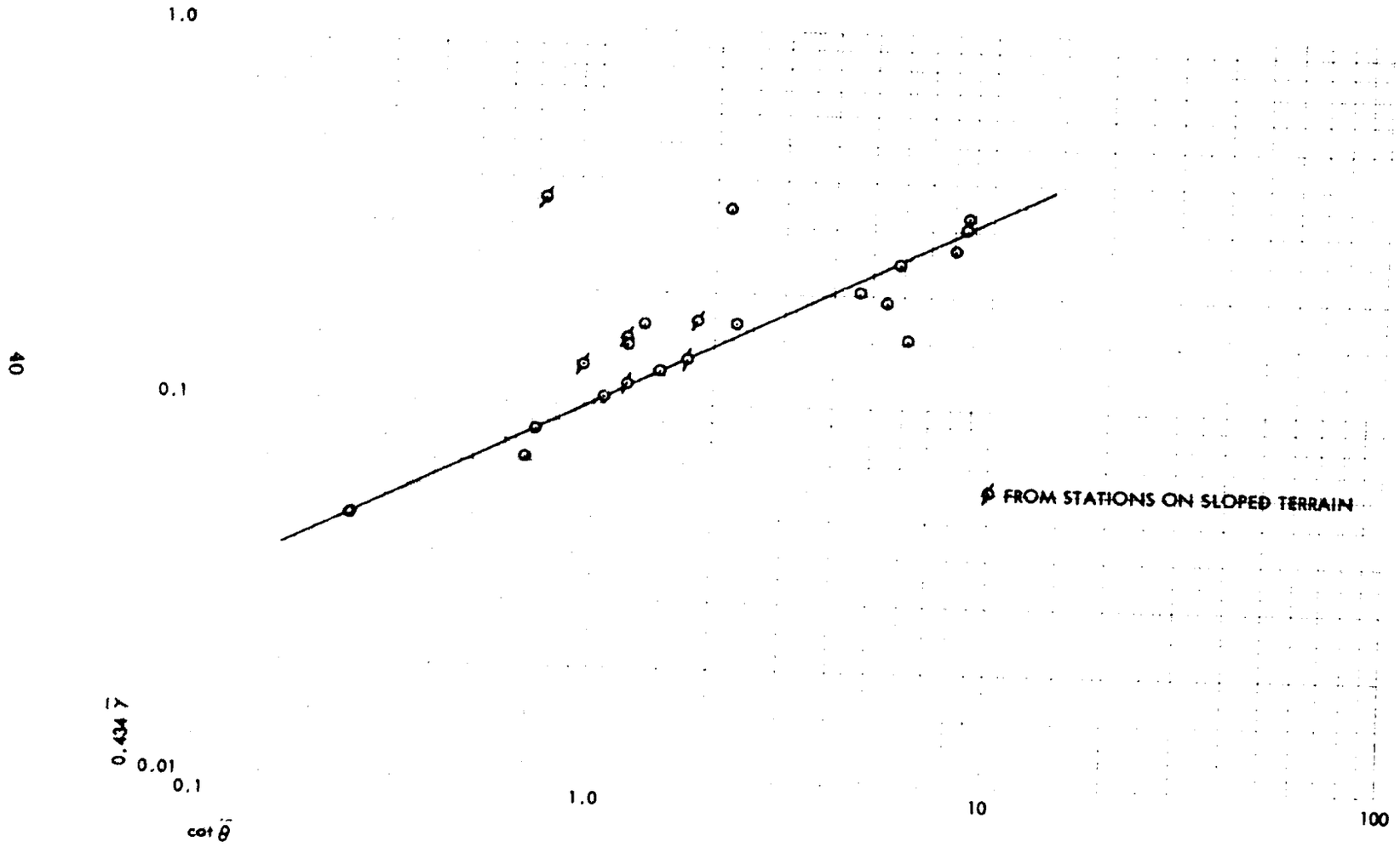

$$\eta(0) = \eta^{o} e^{-\gamma(1 + \cos 2\bar{\varphi})} \tag{12}$$

In analyzing the data for the class two geometry sets, the impaction coefficients for plate angles that are larger than zero degrees were evaluated relative to those for the horizontal plates; the general form of the equation for the impaction coefficient used in the analysis of the data is given by

$$\eta = \frac{(1 + \Delta_t)\ \eta(0)\ \sin(\bar{\varphi} - \theta)}{\sin \bar{\varphi}} \tag{13}$$

in which Δ_t is a correction term whose value depends on $\bar{\varphi}$ and θ in such a way that it becomes zero where θ is zero. Initial plots of the derived values of Δ_t as a function of cot $\bar{\varphi}$ indicated that Δ_t was about proportional to $\cot^2\bar{\varphi}$ and that $\Delta_t/\cot^2\bar{\varphi}$ decreased as $\bar{\varphi} - \theta$ decreased (at least for $\bar{\varphi} - \theta$ values larger than 2 or 3 degrees). An exponential form for representing this decrease of $\Delta_t/\cot^2\bar{\varphi}$ with angular spread was selected; and, since Δ_t must be zero at θ equal to zero, the argument of the exponential must contain the term -cot θ. Further analysis of the data indicated that the calculated values of Δ_t were represented fairly well by

$$\Delta_t = 60.0\ \cot^2\bar{\varphi}\ e^{-2.02\ \cot\theta\ \cot^{1/2}\bar{\varphi}}, \quad \theta \le \bar{\varphi} \tag{14}$$

The calculated values of η/η^{o}, $\Delta_t/\cot^2\bar{\varphi}$, and cot θ $\cot^{1/2}\bar{\varphi}$ for each set at the plate angles of 30 and 60 degrees are summarized in Table 10. The variation of $\Delta_t/\cot^2\bar{\varphi}$ with the argument cot θ $\cot^{1/2}\bar{\varphi}$ is plotted in Figure 8. The large divergence of the point for Set No. 18 could be due either to a small error in the selected value of $\bar{\varphi}$ or to the fact that the distribution of particle diameters would always give high derived values of η/η^{o} and other parameters. If the distribution resulted in a small but measurable value of m where $\bar{\varphi}$ was equal to θ, the derived value of $\Delta_t/\cot^2\bar{\varphi}$ would be infinity.

The overall equation for the deposit density of particles on the plates for the class two geometry is given by

$$m = \frac{\eta^{o} m_a\ (1 + \Delta_t)\ \sin^2(\bar{\varphi} - \theta)\ e^{-\gamma(1 + \cos 2\bar{\varphi})}}{\sin \bar{\varphi}}, \quad \theta \le \bar{\varphi} \tag{15}$$

where γ is given by Equation 11 and Δ_t is given by Equation 14.

Table 10

SUMMARY OF IMPACTION DATA AND PARAMETERS FOR THE CLASS TWO AND FOUR GEOMETRIES

Set Number	$\theta = 30^\circ$				$\theta = 60^\circ$			
	$\bar{\varphi}-\theta$	η/η°	$\Delta_t/\cot^2\bar{\varphi}$ [a]	$\chi(\theta,\bar{\varphi})$ [b]	$\bar{\varphi}-\theta$	η/η°	$\Delta_t/\cot^2\bar{\varphi}$ [a]	$\chi(\theta,\bar{\varphi})$ [b]
2	$-(17^\circ 42')$	0.2271	0.4541	0.5514	$-(47^\circ 42')$	0.09965	0.1151	0.8600
3	$4^\circ 43'$	0.5527	2.208	2.080	-	-	-	-
4	$24^\circ 40'$	1.658	5.350	1.458	$-(5^\circ 20')$	2.898	3.347	0.3049
5	$13^\circ 52'$	1.143	2.979	1.767	$-(16^\circ 08')$	0.5804	0.6702	0.5271
6	$9^\circ 34'$	0.5339	1.381	1.575	-	-	-	-
7	$46^\circ 17'$	0.8504	2.647	0.8557	$16^\circ 17'$	0.8354	32.45	0.2852
8	$7^\circ 04'$	0.8610	3.294	1.994	-	-	-	-
9	$-(6^\circ 00')$	0.3909	0.7818	0.3233	-	-	-	-
11	$-(23^\circ 17')$	0.1066	0.2133	0.6287	-	-	-	-
12	$26^\circ 18'$	0.8159	1.474	1.415	$-(3^\circ 42')$	3.217	3.714	0.2540
13	$-(20^\circ 44')$	0.2109	0.4217	0.5950	$-(50^\circ 44')$	0.1321	0.1525	0.8799
14	$-(20^\circ 15')$	0.1006	0.2012	0.5883	$-(50^\circ 15')$	0.03475	0.04013	0.8768
17	$9^\circ 46'$	1.014	2.911	1.898	$-(20^\circ 14')$	0.3027	0.3495	0.5881
18	$0^\circ 29'$	13.96	543.1	2.257	$-(29^\circ 31')$	0.1293	0.1493	0.7019
19	$17^\circ 01'$	0.5297	0.8488	1.672	$-(12^\circ 59')$	0.2844	0.3284	0.4737
20	$-(10^\circ 12')$	0.07238	0.1448	0.4208	-	-	-	-
21	$-(5^\circ 21')$	0.9183	1.837	0.3053	-	-	-	-
22	$23^\circ 56'$	0.3539	0.4302	1.478	$-(6^\circ 04')$	0.2430	0.2806	0.3251

a For negative values of $(\bar{\varphi}-\theta)$ this heading is $\eta/(\eta^\circ \sin\theta)$, defined as Δ_t' in text

b $\chi(\theta,\bar{\varphi}) = \cot\theta \cot^{1/2}\bar{\varphi}$ for positive values of $(\bar{\varphi}-\theta)$; $\chi(\theta,\bar{\varphi}) = \sin^{1/2}(\theta-\bar{\varphi})$ for negative values of $(\bar{\varphi}-\theta)$

Figure 8

VARIATION OF $\ln (\Delta_t / \cot^2 \bar{\phi})$ WITH $\cot \theta \cot^{\frac{1}{2}} \bar{\phi}$, CLASS TWO GEOMETRY

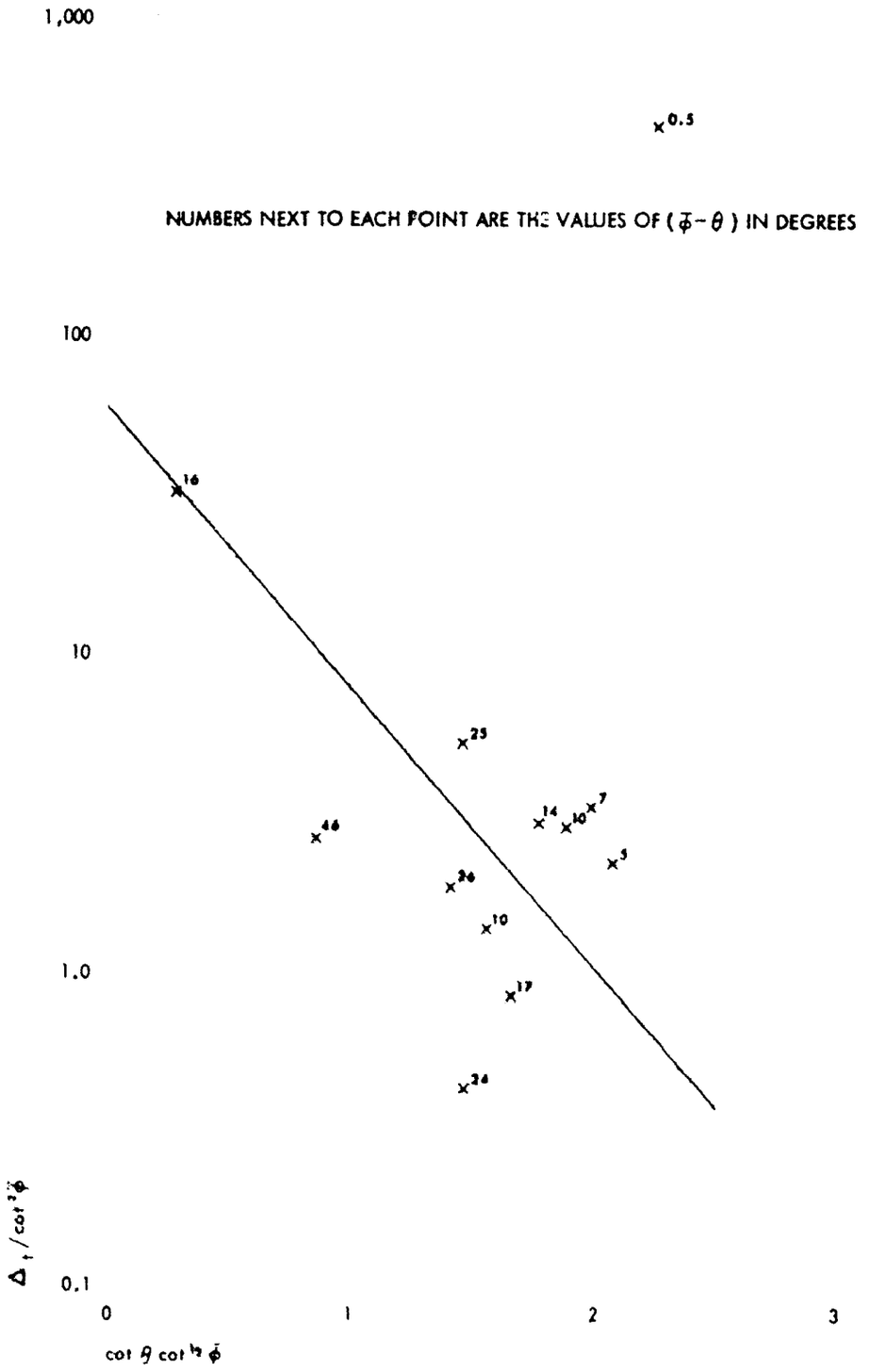

The general equation used for correlating the impaction data for the class four geometry plates is given by

$$\eta = \eta^{o}\Delta_t' \sin\theta, \quad \theta = 0 \text{ to } 90^{o} \tag{16}$$

The data for Δ_t' are plotted as a function of $\sin^{1/2}(\theta - \bar{\varphi})$ in Figure 9; the line drawn through the points is given by

$$\eta^{o}\Delta_t' = 2.0\ e^{-1.05 \sin^{1/2}(\theta - \bar{\varphi})}, \quad \theta \geq \bar{\varphi} \tag{17}$$

so that, for the class four geometry plates, the particle density on a plate is represented by

$$m = 2.0\ \eta^{o}m_a \sin\theta \sin(\theta - \bar{\varphi})\ e^{-1.05 \sin^{1/2}(\theta - \bar{\varphi})}, \quad \theta \geq \bar{\varphi} \tag{18}$$

The value of m in Equation 18 approaches zero as θ approaches zero as it is desired for a single particle diameter and constant wind speed. Under field conditions where the deposit consists of particles with a range in diameters and where some degree of fluctuation in the wind speed occurs over the disposition period, the plates at angles where $\theta - \bar{\varphi}$ is small will usually collect more particles than that estimated from Equations 15 and 18. The relative increase in the deposits as a result of these effects is shown by the scatter diagram of the $\eta/\eta(0)$ values in Figure 10 for $|\theta - \bar{\varphi}|$ values up to 12 degrees where the ratio approaches unity. The correlation line shown in the figure yields the following representation for η (class two and four geometries):

$$\eta = 10.0\ \eta(0)\ e^{-10.5 \sin|\bar{\varphi} - \theta|}, \quad |\bar{\varphi} - \theta| \leq 12^{o} \tag{19}$$

Thus for the impaction of particles with a distribution of diameters, the value of η for deposits on the top side of the plates, when θ is within 12 degrees of $\bar{\varphi}$, is estimated from Equation 19 instead of 15 and 18 for both the class two and class four geometries.

The impaction data for the class three geometry plates, where the particles impact the undersides of the plates between 0 and 90 degrees, are summarized in Table 11; the data for the plates at 30 and 60 degrees were correlated by comparison with the impaction coefficient of the plate at 90 degrees using the general expression

Figure 9

VARIATION OF $\ln \Delta_t'$ WITH $\sin^{\frac{1}{2}}(\theta - \bar{\phi})$, CLASS FOUR GEOMETRY

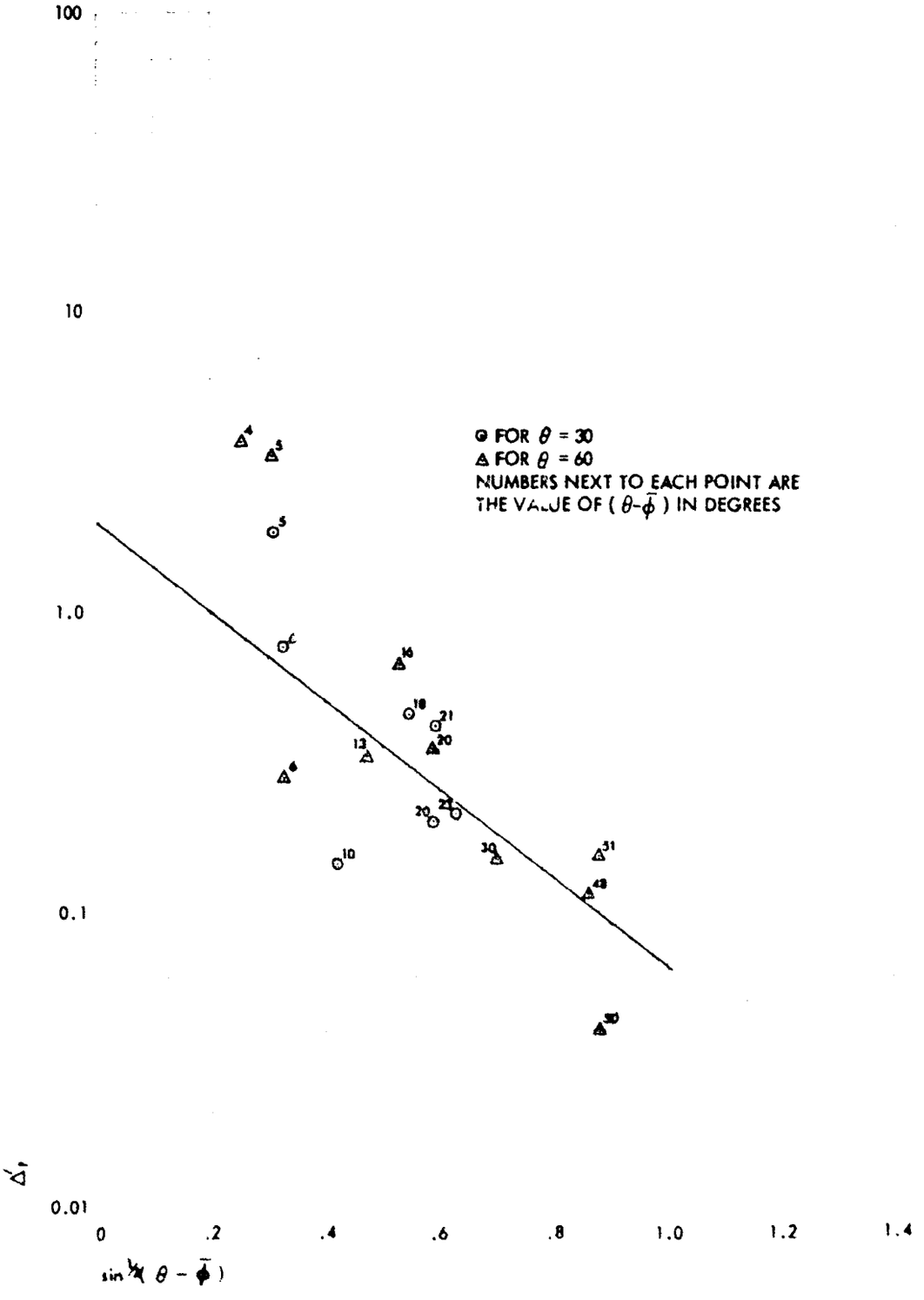

Figure 10

VARIATION OF $\ln[\eta/\eta(0)]$ WITH $\sin|\bar{\phi}-\theta|$ FOR LOW VALUES OF $|\bar{\phi}-\theta|$

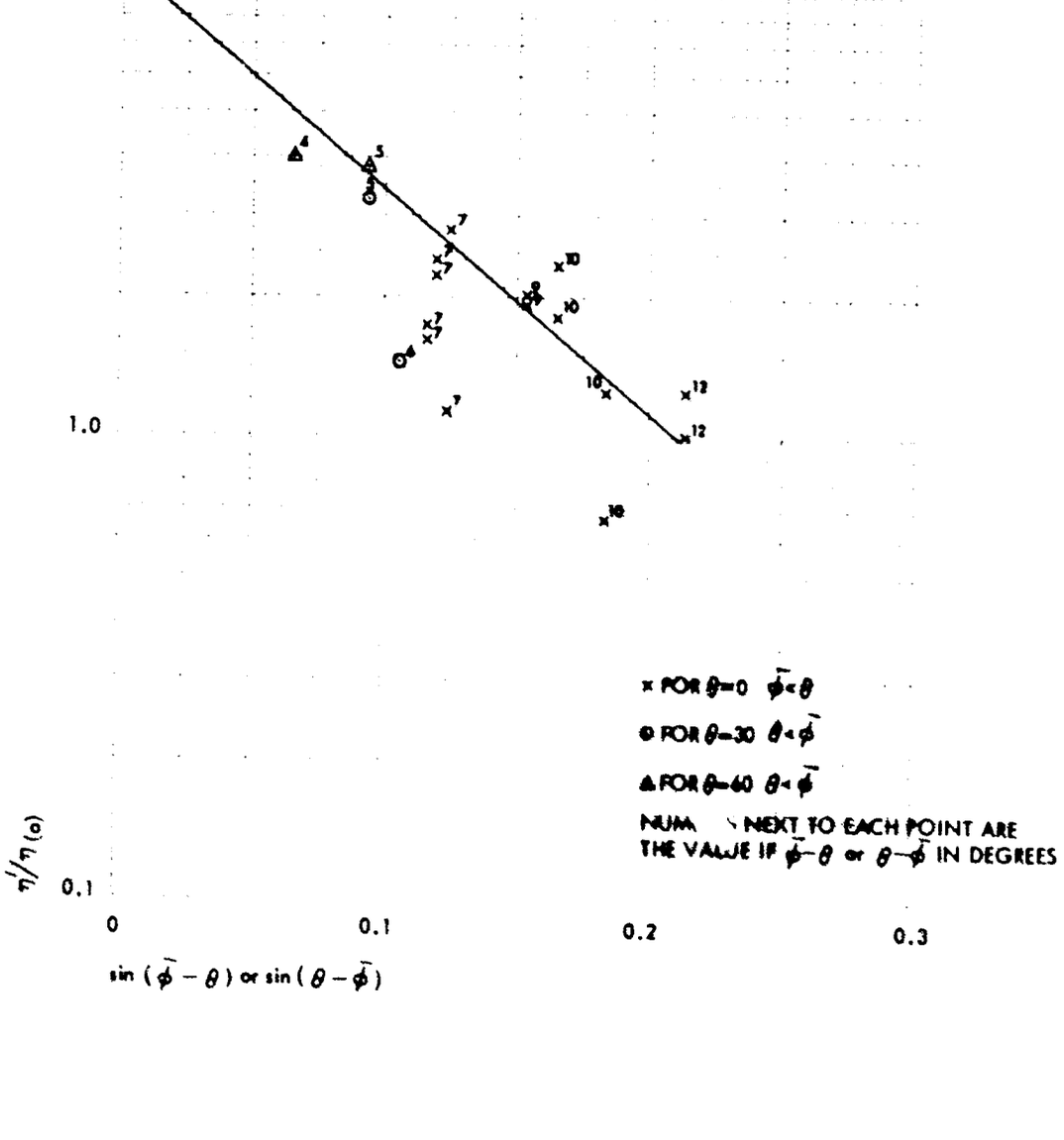

Table 11

SUMMARY OF IMPACTION DATA AND PARAMETERS FOR THE CLASS THREE GEOMETRY

Set Number	$\theta = 30^\circ$				$\theta = 60^\circ$			
	$\theta-\bar{\varphi}$	η/η°	$\Delta_b \cot^2 \bar{\varphi}$	$\chi(\theta,\bar{\varphi})^a$	$\theta-\bar{\varphi}$	η/η°	$\Delta_b \cot^2 \bar{\varphi}$	$\chi(\theta,\bar{\varphi})^a$
1	19°31'	0.1562	5.543	0.2605	49°31'	0.7224	10.26	0.7813
2	17°42'	0.8386	95.40	0.2695	47°42'	0.7580	4.250	0.8086
3	-(4°43')	0.5527	-	0.2868	25°17'	0.7183	1.934	1.442
4	-(24°40')	0.09149	-	0.6460	5°20'	1.048	5.854	2.057
5	-(13°52')	0.1640	-	0.4896	16°08'	0.6658	1.799	1.698
6	-	-	-	-	26°26'	0.5160	0.7087	1.575
7	-	-	-	-	-(16°17')	0.05361	-	0.5295
8	-(7°04')	0.1208	-	0.3508	22°56'	0.3836	0.3159	1.505
9	6°00'	0.5103	44.38	0.3852	36°00'	0.5285	0.3669	1.156
10	5°09'	0.6000	58.40	0.3929	35°09'	0.3957	-0.2313	1.179
11	23°17'	0.1275	-24.76	0.1981	53°17'	0.4575	-23.74	0.5944
12	-	-	-	-	3°42'	0.9785	7.133	2.121
13	20°44'	0.2259	10.56	0.2332	50°44'	0.4696	-11.08	0.6996
14	20°15'	0.3392	33.10	0.2339	50°15'	0.8162	8.230	0.7016
15	22°54'	0.4230	76.36	0.2038	52°54'	0.7606	7.192	0.6113
16	23°23'	0.3465	56.42	0.1966	53°23'	0.7275	4.423	0.5900
17	-(9°46')	0.07268	-	0.4118	20°14'	0.4029	0.4250	1.580
18	-(0°29')	3.268	-	0.09188	29°31'	0.5474	0.8308	1.329
19	-	-	-	-	12°59'	0.4675	1.152	1.795
20	10°12'	0.9019	71.07	0.3464	40°12'	0.7345	2.626	1.039
21	5°21'	0.7256	69.27	0.3911	35°21'	0.6714	1.724	1.173
22	-(23°56')	0.02105	-	0.6369	6°04'	0.2702	1.249	2.030

a $\chi(\theta,\bar{\varphi}) = \tan\theta \tan^{1/2}\bar{\varphi}$ for positive values of $(\theta-\bar{\varphi})$; $\chi(\theta,\bar{\varphi}) = \sin^{1/2}(\bar{\varphi}-\theta)$ for negative values of $(\theta-\bar{\varphi})$

$$\eta = \eta^o \sin(\theta - \bar{\varphi}) \sin\theta \left[\frac{\eta(90)}{\eta^o \cos\bar{\varphi}} + \Delta_b\right], \quad \theta \geq \bar{\varphi} \tag{20}$$

in which

$$\eta(90) = \eta^o e^{-\gamma(1 - \cos 2\bar{\varphi})} \tag{21}$$

and Δ_b is a correction term whose value must approach zero as θ approaches 90 degrees. Analysis of the data indicated that Δ_b varied inversely with $\cos^2\bar{\varphi}$; the exponential decrease of the product $\Delta_b \cot^2\bar{\varphi}$ with the argument $\tan\theta \tan^{1/2}\bar{\varphi}$ is shown in Figure 11. The regression line shown in the figure yields the following representation for Δ_b

$$\Delta_b = \frac{90.0\ e^{-3.39 \tan\theta \tan^{1/2}\bar{\varphi}}}{\cot^2\bar{\varphi}}, \quad \theta \geq \bar{\varphi} \tag{22}$$

The scatter diagram of the impaction coefficients for particle deposits on the bottom side of the plates at small values of $\theta - \bar{\varphi}$ and for impactions where $\bar{\varphi} > \theta$ is plotted in Figure 12 as a function of $\sin^{1/2}|\theta - \bar{\varphi}|$. The regression line is represented by

$$\eta = 6.8\ \eta^o\ e^{-8.05 \sin^{1/2}|\bar{\varphi} - \theta|}, \quad |\bar{\varphi} - \theta| \leq 6^o \tag{23}$$

Thus, for impaction of particles with a distribution in diameters, the value of η for deposits on the bottom side of the plates, when θ is within 6 degrees of $\bar{\varphi}$, is estimated from Equation 23 rather than Equation 20 for the class three geometry.

Although no absolute collector was available for calibrating the plate collector system for evaluation of η^o (η^o represents the impaction coefficient of the plate whose plane is perpendicular to the average fall vector of the particles), an approximate evaluation of η^o was made by using the tray collector as a reference standard. And, since the efficiency of the tray collector set at ground level has been established to be very close to 100 percent for particles with diameters of about 100 to 300 microns in wind speeds of 0.5 to 5 feet per second, the correlation of the plate collector and tray collector data would, in effect, relate the impaction coefficients of the plates to the collecting efficiency of the ground.

The estimated values of η^o, relative to the collecting efficiency of the tray collector, and the computed values of the effective average

Figure 11

VARIATION OF $\ln \Delta_b \cot^2 \bar{\phi}$ WITH $\tan^{\frac{1}{2}} \bar{\phi}$, CLASS THREE GEOMETRY

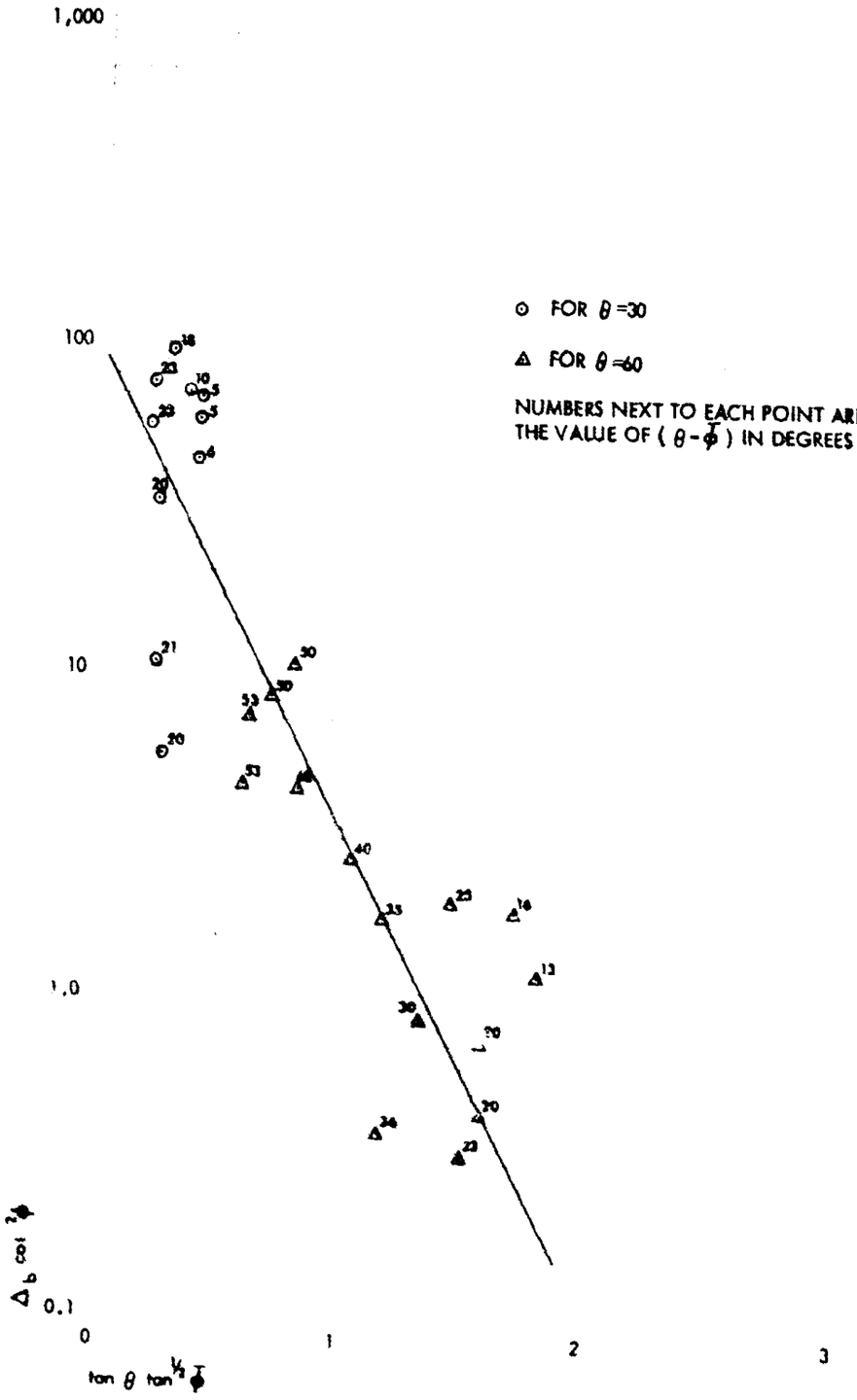

Figure 12

VARIATION OF $\ln(\eta/\eta^{o})$ WITH $\sin^{\frac{1}{2}}|\bar{\phi}-\theta|$, CLASS THREE GEOMETRY

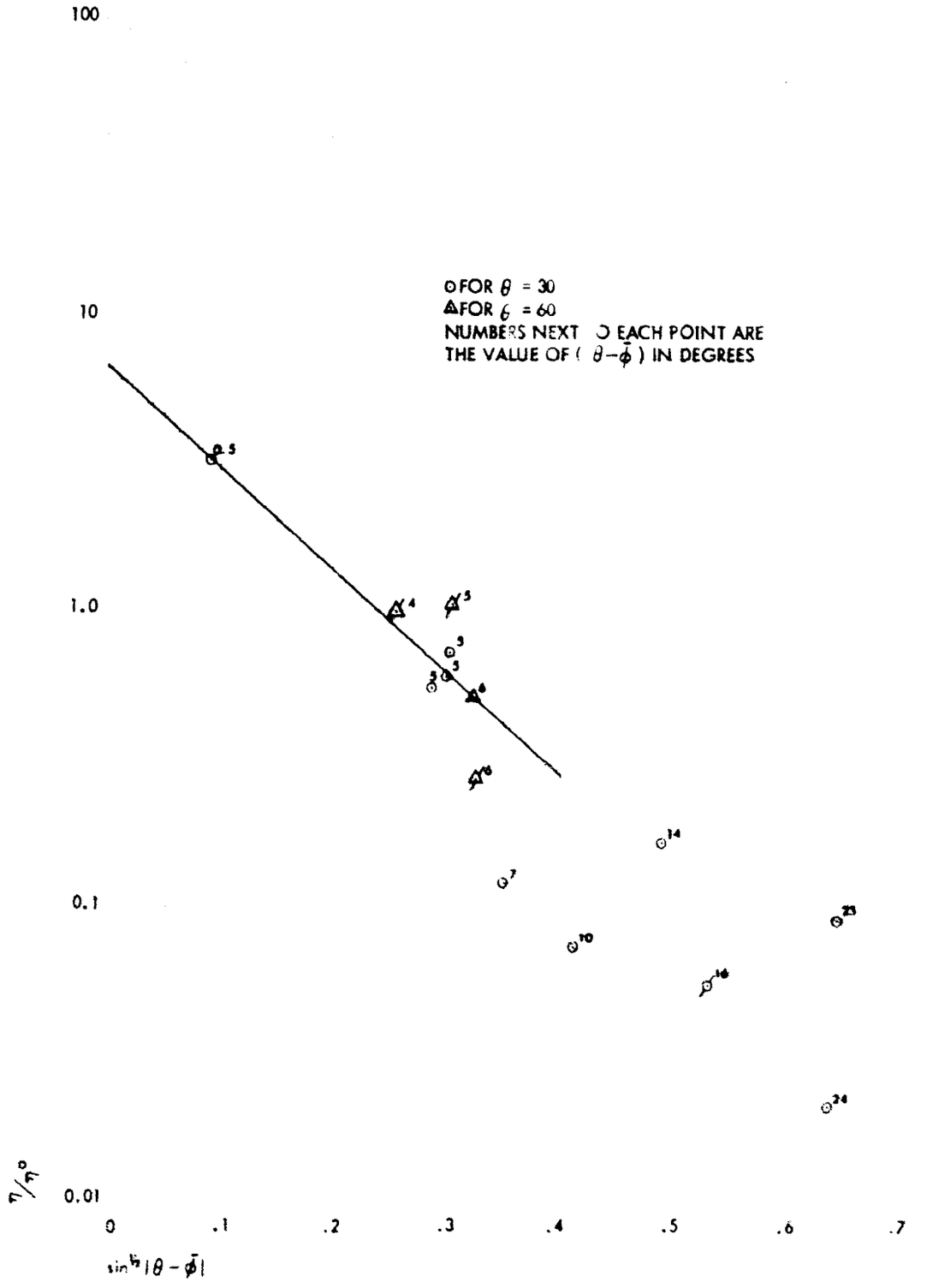

diameter of the particles, $\bar{d}_v$, are summarized in Table 12. The computed values of η^o are plotted as a function of $\bar{v}_w^o/\bar{v}_f^o$ (or cot $\bar{\varphi}$) in Figure 13.

The line drawn through the data points is given by

$$\eta^o = \bar{v}_f^o/\bar{v}_w^o = \tan \bar{\varphi} \qquad (24)$$

The data of Figure 13 indicate that the two collectors (i.e., the tray and the plate that is perpendicular to the average fall vector of the particles) have the same impaction or collecting efficiency when the fall vector is at 45 degrees from the horizontal. The limit of reliability of Equation 24 (and the data of Figure 13) is probably limited to $\bar{v}_w^o/\bar{v}_f^o$ values that range from about 0.5 to 5.0 and to the $\bar{v}_f^o$ values associated with particles whose diameters range from about 30 to 500 microns. It is unlikely that the collecting efficiency of the perpendicular plate, relative to that of the tray collector, would increase indefinitely as the wind speed decreases or as the particle fall velocity increases. Nor is it likely that the relative collecting efficiency of the perpendicular plate would decrease indefinitely as the wind speed increases or the particle fall velocity decreases. More probably, the efficiency of both collectors would approach unity as the wind speed approaches zero, and the relative efficiency of the perpendicular plate would become greater than one at larger values of $\bar{v}_w^o/\bar{v}_f^o$. However, as previously discussed, the absolute value of η^o should become zero for small particles for a given wind speed.

The variation of the mass median diameter of the particles recovered from the tray collectors with the effective average diameters of the falling particles, as computed from the plate collector data, is plotted in Figure 14. The line drawn in the figure represents the relationship that would be expected for the deposition of discrete solid particles. Although some error exists in the computed $\bar{d}_v$ values because of an error in the estimated values of $\bar{\varphi}$ and uncertainties in the associated wind speeds, the expected relationship for solid particles is indicated for only two sets (one point above the curve required an estimate of the vertical component of the wind speed). In all other sets, the value of d_{50} from the sieve analysis is much lower than the computed value of $\bar{d}_v$. In these sets, the particles that fell were therefore agglomerated particles that broke apart either on impact with the plate or in the process of sieving. The extreme case of agglomeration, from the data of Figure 14, is for a $\bar{d}_v$ value of 305 microns and a d_{50} value of 54 microns.

Table 12

ESTIMATES OF η^o RELATIVE TO THE TRAY COLLECTOR EFFICIENCY AND ESTIMATED EFFECTIVE AVERAGE DIAMETER OF THE PARTICLES

Set Number	$\bar{v}^o_w/\bar{v}^o_f$	$\bar{v}^o_f$ (ft/sec)	m_o (gm/sq ft)	η^o	$\bar{d}_v$ (microns)
1	5.40	1.11	0.7238	0.503	63
2	4.59	1.59	1.97	0.369	80
3	1.44	5.90	0.1823	0.531	220
4	0.709	2.68	0.1848	1.26	120
5	1.04	2.21	0.2294	1.06	105
6	1.21	2.89	30.00	1.05	125
7	0.244	8.20	0.128	4.00	305
8	1.32	5.38	1.03	0.562	205
9	2.25	4.31	1.03	0.622	170
10	2.16	6.11	0.714	0.554	230
11	8.49	1.65	3.42	0.121	82
12	0.667	8.10	0.120	1.06	305
13	6.13	1.94	0.807	0.256	93
14	5.82	1.58	0.709	0.174	80
15	8.01	1.80	1.13	0.262	87
16	8.62	1.72	1.21	0.357	84
17	1.20	2.41	2.630	0.944	110
18	1.70	6.59	1.768	0.790	245
19	0.932	2.94	0.3069	0.817	130
20	2.78	4.11	2.356	0.424	160
21	2.18	3.46	0.8421	0.225	140
22	0.728	0.480	0.9556	1.68	39

Figure 13

VARIATION OF COMPUTED VALUES OF η° RELATIVE TO TRAY COLLECTOR WITH $\bar{v}_w^{\circ}/\bar{v}_f^{\circ}$

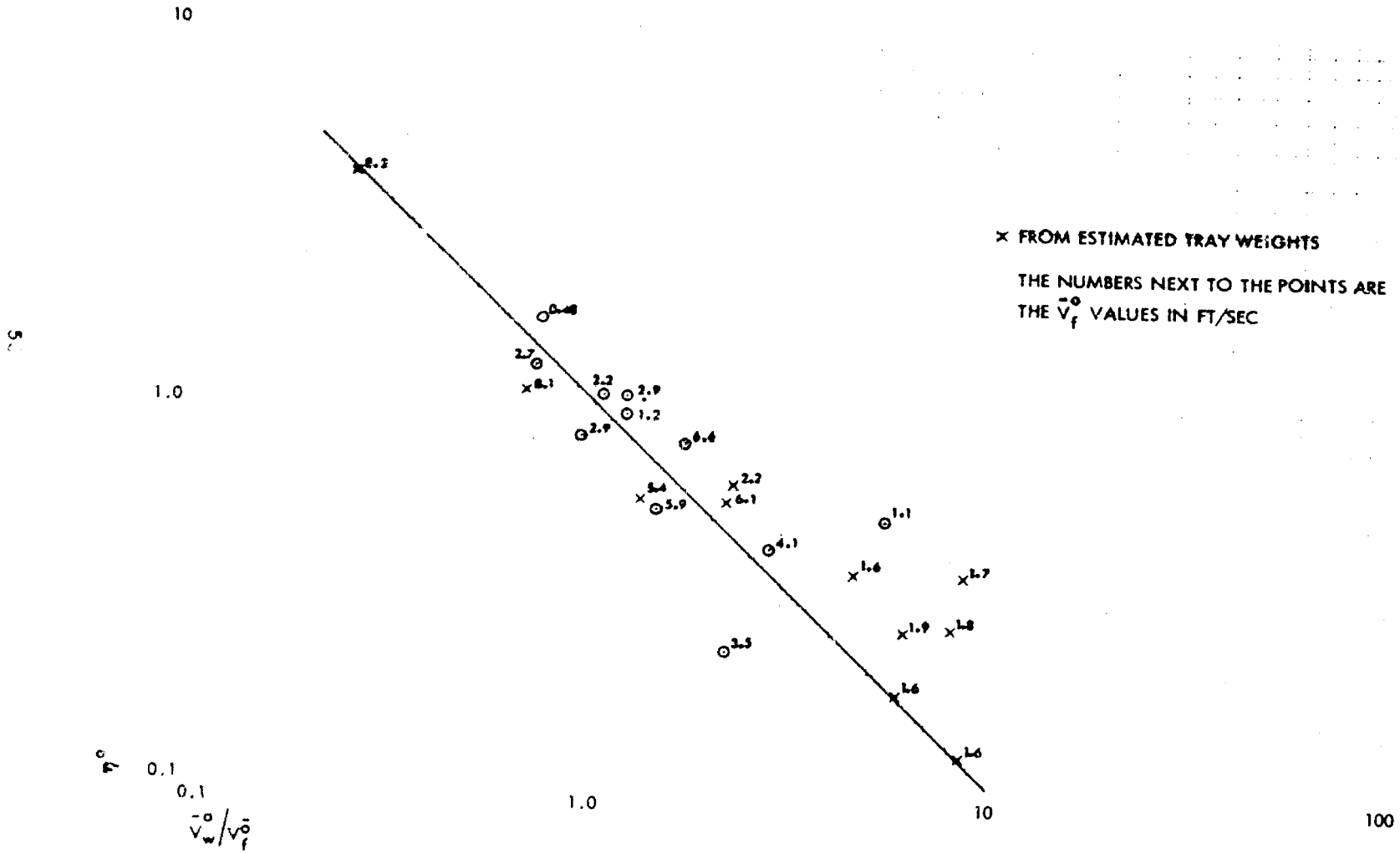

Figure 14

VARIATION OF d_{50} FROM SIEVE ANALYSIS OF TRAY COLLECTOR SAMPLES WITH COMPUTED VALUES OF $\bar{d}_v$

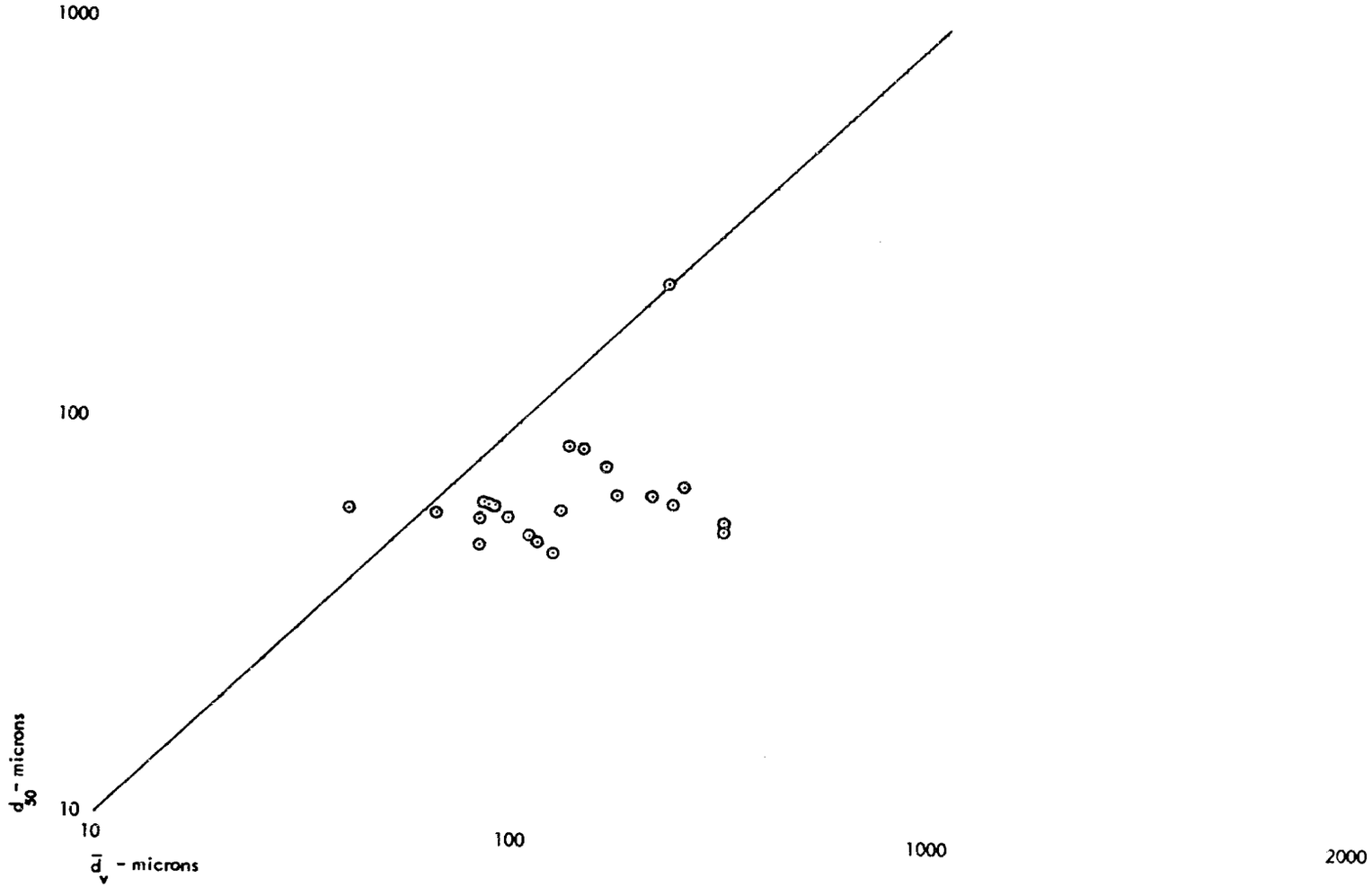

SUMMARY AND CONCLUSIONS

Impaction data for a plate collector exposed to falling particles that were produced by explosive eruptions of volcano Irazú were correlated, and approximating functions for representing the impaction coefficients of the plates were derived from the data. The arrangement of the plates at 0 (180), 30, 60, 90, 120, and 150 degrees from the horizontal provided four classes of impaction geometries.

An approximate relationship between the impaction or collecting efficiency of the plates and the tray collector (or the ground surface) was also derived.

The plate collector data were used to estimate the effective average diameter of the falling particles, and, with a few exceptions, this diameter was always greater than the mass median diameter determined from sieve analysis of the particles. Thus it was concluded that, in the majority of the particle showers, the particles fell and impacted as agglomerates of many smaller particles.

REFERENCES

1. Miller, Carl F., and Hong Lee, Operation Ceniza-Arena: The Retention of Fallout Particles from Volcán Irazú (Costa Rica) by Plants and People, Part One, Stanford Research Institute, Project No. MU-4890, January 1966

2. Miller, Carl F., Operation Ceniza-Arena: The Retention of Fallout Particles from Volcán Irazú (Costa Rica) by Plants and People, Part Two, Stanford Research Institute, Project No. MU-4890, December 1966

3. Miller, Carl F., The Contamination Behavior of Fallout-Like Particles Ejected by Volcano Irazú, Stanford Research Institute, Project No. MU-5779, April 1966

4. Ranz, W. E., and J. B. Wong, "Impaction of Dust and Smoke Particles on Surface and Body Collectors," Ind. Eng. Chem., 44, 1371-1381 (1952)

TITLE: The Impaction of Airborne Particles on Plate Collectors

By: Carl F. Miller

SUMMARY:

Impaction data for a plate collector exposed to falling particles that were produced by explosive eruptions of volcano Irazú were correlated, and approximating functions for representing the impaction coefficients of the plates were derived from the data. The arrangement of the plates at 0 (180), 30, 60, 90, 120, and 150 degrees from the horizontal provided four classes of impaction geometries.

An approximate relationship between the impaction or collecting efficiency of the plates and the tray collector (or the ground surface) was also derived.

The plate collector data were used to estimate the effective average diameter of the falling particles, and, with a few exceptions, this diameter was always greater than the mass median diameter determined from sieve analysis of the particles. Thus it was concluded that, in the majority of the particle showers, the particles fell and impacted as agglomerates of many smaller particles.

SRI Project No. MU-6358 April 1967

Contract No. NOO22867C1143
OCD Work Unit No. 3119A

TITLE: The Impaction of Airborne Particles on Plate Collectors

By: Carl F. Miller

SUMMARY:

Impaction data for a plate collector exposed to falling particles that were produced by explosive eruptions of volcano Irazú were correlated, and approximating functions for representing the impaction coefficients of the plates were derived from the data. The arrangement of the plates at 0 (180), 30, 60, 90, 120, and 150 degrees from the horizontal provided four classes of impaction geometries.

An approximate relationship between the impaction or collecting efficiency of the plates and the tray collector (or the ground surface) was also derived.

The plate collector data were used to estimate the effective average diameter of the falling particles, and, with a few exceptions, this diameter was always greater than the mass median diameter determined from sieve analysis of the particles. Thus it was concluded that, in the majority of the particle showers, the particles fell and impacted as agglomerates of many smaller particles.

SRI Project No. MU-6358 April 1967

Contract No. NOO22867C1143
OCD Work Unit No. 3119A

UNCLASSIFIED
Security Classification

DOCUMENT CONTROL DATA - R&D
(Security classification of title, body of abstract and indexing annotation must be entered when the overall report is classified)

1 ORIGINATING ACTIVITY (Corporate author) STANFORD RESEARCH INSTITUTE Menlo Park, California 94025	2a REPORT SECURITY CLASSIFICATION UNCLASSIFIED 2b GROUP

3 REPORT TITLE

THE IMPACTION OF AIRBORNE PARTICLES ON PLATE COLLECTORS

4 DESCRIPTIVE NOTES (Type of report and inclusive dates)

5 AUTHOR(S) (Last name, first name, initial)

MILLER, Carl F.

6 REPORT DATE	7a TOTAL NO OF PAGES	7b NO OF REFS
April 1967	56	4

8a CONTRACT OR GRANT NO NO022867C1143 b PROJECT NO OCD Work Unit No. 3119A c SRI Project No. MU-6358 d	9a ORIGINATOR'S REPORT NUMBER(S) 9b OTHER REPORT NO(S) (Any other numbers that may be assigned this report)

10 AVAILABILITY LIMITATION NOTICES

Distribution of this document is unlimited.

11 SUPPLEMENTARY NOTES	12 SPONSORING MILITARY ACTIVITY
	Office of Civil Defense Department of the Army Washington, D.C. 20310

13 ABSTRACT

Impaction data for a plate collector exposed to falling particles that were produced by explosive eruptions of volcano Irazú were correlated, and approximating functions for representing the impaction coefficients of the plates were derived from the data. The arrangement of the plates at 0 (180), 30, 60, 90, 120, and 150 degrees from the horizontal provided four classes of impaction geometries.

An approximate relationship between the impaction or collecting efficiency of the plates and the tray collector (or the ground surface) was also derived.

The plate collector data were used to estimate the effective average diameter of the falling particles, and, with a few exceptions, this diameter was always greater than the mass median diameter determined from sieve analysis of the particles. Thus it was concluded that, in the majority of the particle showers, the particles fell and impacted as agglomerates of many smaller particles.

DD FORM 1 JAN 64 1473

UNCLASSIFIED
Security Classification

14 KEY WORDS	LINK A		LINK B		LINK C	
	ROLE	WT	ROLE	WT	ROLE	WT
Plate collector						
Particle impaction						
Particles						
Volcano Irazú						
Greased plates						
Particle trajectory						
Particle retention						
Volcanic dust						

INSTRUCTIONS

1. ORIGINATING ACTIVITY: Enter the name and address of the contractor, subcontractor, grantee, Department of Defense activity or other organization *(corporate author)* issuing the report.

2a. REPORT SECURITY CLASSIFICATION: Enter the overall security classification of the report. Indicate whether "Restricted Data" is included. Marking is to be in accordance with appropriate security regulations.

2b. GROUP: Automatic downgrading is specified in DoD Directive 5200.10 and Armed Forces Industrial Manual. Enter the group number. Also, when applicable, show that optional markings have been used for Group 3 and Group 4 as authorized.

3. REPORT TITLE: Enter the complete report title in all capital letters. Titles in all cases should be unclassified. If a meaningful title cannot be selected without classification, show title classification in all capitals in parenthesis immediately following the title.

4. DESCRIPTIVE NOTES: If appropriate, enter the type of report, e.g., interim, progress, summary, annual, or final. Give the inclusive dates when a specific reporting period is covered.

5. AUTHOR(S): Enter the name(s) of author(s) as shown on or in the report. Enter last name, first name, middle initial. If military, show rank and branch of service. The name of the principal author is an absolute minimum requirement.

6. REPORT DATE: Enter the date of the report as day, month, year, or month, year. If more than one date appears on the report, use date of publication.

7a. TOTAL NUMBER OF PAGES: The total page count should follow normal pagination procedures, i.e., enter the number of pages containing information.

7b. NUMBER OF REFERENCES: Enter the total number of references cited in the report.

8a. CONTRACT OR GRANT NUMBER: If appropriate, enter the applicable number of the contract or grant under which the report was written.

8b, 8c, & 8d. PROJECT NUMBER: Enter the appropriate military department identification, such as project number, subproject number, system numbers, task number, etc.

9a. ORIGINATOR'S REPORT NUMBER(S): Enter the official report number by which the document will be identified and controlled by the originating activity. This number must be unique to this report.

9b. OTHER REPORT NUMBER(S): If the report has been assigned any other report numbers *(either by the originator or by the sponsor)*, also enter this number(s).

10. AVAILABILITY/LIMITATION NOTICES: Enter any limitations on further dissemination of the report, other than those imposed by security classification, using standard statements such as:

(1) "Qualified requesters may obtain copies of this report from DDC."

(2) "Foreign announcement and dissemination of this report by DDC is not authorized."

(3) "U. S. Government agencies may obtain copies of this report directly from DDC. Other qualified DDC users shall request through _____ _____."

(4) "U. S. military agencies may obtain copies of this report directly from DDC. Other qualified users shall request through _____."

(5) "All distribution of this report is controlled. Qualified DDC users shall request through _____."

If the report has been furnished to the Office of Technical Services, Department of Commerce, for sale to the public, indicate this fact and enter the price, if known.

11. SUPPLEMENTARY NOTES: Use for additional explanatory notes.

12. SPONSORING MILITARY ACTIVITY: Enter the name of the departmental project office or laboratory sponsoring *(paying for)* the research and development. Include address.

13. ABSTRACT: Enter an abstract giving a brief and factual summary of the document indicative of the report, even though it may also appear elsewhere in the body of the technical report. If additional space is required, a continuation sheet shall be attached.

It is highly desirable that the abstract of classified reports be unclassified. Each paragraph of the abstract shall end with an indication of the military security classification of the information in the paragraph, represented as (TS), (S), (C), or (U).

There is no limitation on the length of the abstract. However, the suggested length is from 150 to 225 words.

14. KEY WORDS: Key words are technically meaningful terms or short phrases that characterize a report and may be used as index entries for cataloging the report. Key words must be selected so that no security classification is required. Identifiers, such as equipment model designation, trade name, military project code name, geographic location, may be used as key words but will be followed by an indication of technical context. The assignment of links, roles, and weights is optional.

DD FORM 1 JAN 64 1473 (BACK)